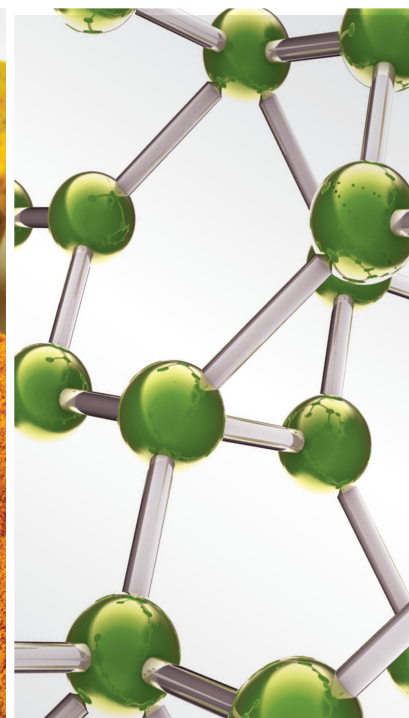
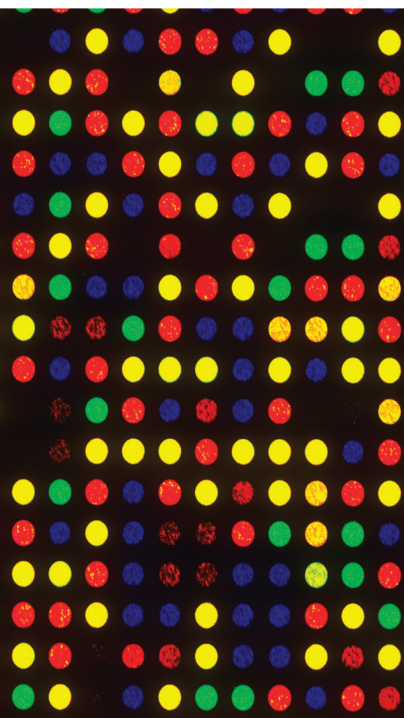


Biotechnology and Therapeutic Applications of Medicinal Plants for Viral Infections

Lead Guest Editor: Zheng Feei Ma

Guest Editors: Xiaoqin Luo and Zhongxiao Wan





Biotechnology and Therapeutic Applications of Medicinal Plants for Viral Infections

Evidence-Based Complementary and Alternative Medicine

**Biotechnology and Therapeutic
Applications of Medicinal Plants for
Viral Infections**

Lead Guest Editor: Zheng Feei Ma

Guest Editors: Xiaoqin Luo and Zhongxiao Wan



Copyright © 2021 Hindawi Limited. All rights reserved.

This is a special issue published in "Evidence-Based Complementary and Alternative Medicine." All articles are open access articles distributed under the Creative Commons Attribution License, which permits unrestricted use, distribution, and reproduction in any medium, provided the original work is properly cited.

Chief Editor

Jian-Li Gao , China

Associate Editors

Hyunsu Bae , Republic of Korea
Raffaele Capasso , Italy
Jae Youl Cho , Republic of Korea
Caigan Du , Canada
Yuewen Gong , Canada
Hai-dong Guo , China
Kuzhuvelil B. Harikumar , India
Ching-Liang Hsieh , Taiwan
Cheorl-Ho Kim , Republic of Korea
Victor Kuete , Cameroon
Hajime Nakae , Japan
Yoshiji Ohta , Japan
Olumayokun A. Olajide , United Kingdom
Chang G. Son , Republic of Korea
Shan-Yu Su , Taiwan
Michał Tomczyk , Poland
Jenny M. Wilkinson , Australia

Academic Editors

Eman A. Mahmoud , Egypt
Ammar AL-Farga , Saudi Arabia
Smail Aazza , Morocco
Nahla S. Abdel-Azim, Egypt
Ana Lúcia Abreu-Silva , Brazil
Gustavo J. Acevedo-Hernández , Mexico
Mohd Adnan , Saudi Arabia
Jose C Adsuar , Spain
Sayeed Ahmad, India
Touqeer Ahmed , Pakistan
Basiru Ajiboye , Nigeria
Bushra Akhtar , Pakistan
Fahmida Alam , Malaysia
Mohammad Jahoor Alam, Saudi Arabia
Clara Albani, Argentina
Ulysses Paulino Albuquerque , Brazil
Mohammed S. Ali-Shtayeh , Palestinian Authority
Ekram Alias, Malaysia
Terje Alraek , Norway
Adolfo Andrade-Cetto , Mexico
Letizia Angiolella , Italy
Makoto Arai , Japan

Daniel Dias Rufino Arcanjo , Brazil
Duygu AĞAGÜNDÜZ , Turkey
Neda Baghban , Iran
Samra Bashir , Pakistan
Rusliza Basir , Malaysia
Jairo Kenupp Bastos , Brazil
Arpita Basu , USA
Mateus R. Beguelini , Brazil
Juana Benedí, Spain
Samira Boulbaroud, Morocco
Mohammed Bourhia , Morocco
Abdelhakim Bouyahya, Morocco
Nunzio Antonio Cacciola , Italy
Francesco Cardini , Italy
María C. Carpinella , Argentina
Harish Chandra , India
Guang Chen, China
Jianping Chen , China
Kevin Chen, USA
Mei-Chih Chen, Taiwan
Xiaojia Chen , Macau
Evan P. Cherniack , USA
Giuseppina Chianese , Italy
Kok-Yong Chin , Malaysia
Lin China, China
Salvatore Chirumbolo , Italy
Hwi-Young Cho , Republic of Korea
Jeong June Choi , Republic of Korea
Jun-Yong Choi, Republic of Korea
Kathrine Bisgaard Christensen , Denmark
Shuang-En Chuang, Taiwan
Ying-Chien Chung , Taiwan
Francisco José Cidral-Filho, Brazil
Daniel Collado-Mateo , Spain
Lisa A. Conboy , USA
Kieran Cooley , Canada
Edwin L. Cooper , USA
José Otávio do Amaral Corrêa , Brazil
Maria T. Cruz , Portugal
Huantian Cui , China
Giuseppe D'Antona , Italy
Ademar A. Da Silva Filho , Brazil
Chongshan Dai, China
Laura De Martino , Italy
Josué De Moraes , Brazil

Arthur De Sá Ferreira , Brazil
Nunziatina De Tommasi , Italy
Marinella De leo , Italy
Gourav Dey , India
Dinesh Dhamecha, USA
Claudia Di Giacomo , Italy
Antonella Di Sotto , Italy
Mario Dioguardi, Italy
Jeng-Ren Duann , USA
Thomas Efferth , Germany
Abir El-Alfy, USA
Mohamed Ahmed El-Esawi , Egypt
Mohd Ramli Elvy Suhana, Malaysia
Talha Bin Emran, Japan
Roger Engel , Australia
Karim Ennouri , Tunisia
Giuseppe Esposito , Italy
Tahereh Eteraf-Oskouei, Iran
Robson Xavier Faria , Brazil
Mohammad Fattahi , Iran
Keturah R. Faurot , USA
Piergiorgio Fedeli , Italy
Laura Ferraro , Italy
Antonella Fioravanti , Italy
Carmen Formisano , Italy
Hua-Lin Fu , China
Liz G Müller , Brazil
Gabino Garrido , Chile
Safoora Gharibzadeh, Iran
Muhammad N. Ghayur , USA
Angelica Gomes , Brazil
Elena González-Burgos, Spain
Susana Gorzalczany , Argentina
Jiangyong Gu , China
Maruti Ram Gudavalli , USA
Jian-You Guo , China
Shanshan Guo, China
Narcís Gusi , Spain
Svein Haavik, Norway
Fernando Hallwass, Brazil
Gajin Han , Republic of Korea
Ihsan Ul Haq, Pakistan
Hicham Harhar , Morocco
Mohammad Hashem Hashempur , Iran
Muhammad Ali Hashmi , Pakistan

Waseem Hassan , Pakistan
Sandrina A. Heleno , Portugal
Pablo Herrero , Spain
Soon S. Hong , Republic of Korea
Md. Akil Hossain , Republic of Korea
Muhammad Jahangir Hossen , Bangladesh
Shih-Min Hsia , Taiwan
Changmin Hu , China
Tao Hu , China
Weicheng Hu , China
Wen-Long Hu, Taiwan
Xiao-Yang (Mio) Hu, United Kingdom
Sheng-Teng Huang , Taiwan
Ciara Hughes , Ireland
Attila Hunyadi , Hungary
Liaquat Hussain , Pakistan
Maria-Carmen Iglesias-Osma , Spain
Amjad Iqbal , Pakistan
Chie Ishikawa , Japan
Angelo A. Izzo, Italy
Satveer Jagwani , USA
Rana Jamous , Palestinian Authority
Muhammad Saeed Jan , Pakistan
G. K. Jayaprakasha, USA
Kyu Shik Jeong, Republic of Korea
Leopold Jirovetz , Austria
Jeeyoun Jung , Republic of Korea
Nurkhalida Kamal , Saint Vincent and the
Grenadines
Atsushi Kameyama , Japan
Kyungsu Kang, Republic of Korea
Wenyi Kang , China
Shao-Hsuan Kao , Taiwan
Nasiara Karim , Pakistan
Morimasa Kato , Japan
Kumar Katragunta , USA
Deborah A. Kennedy , Canada
Washim Khan, USA
Bonglee Kim , Republic of Korea
Dong Hyun Kim , Republic of Korea
Junghyun Kim , Republic of Korea
Kyungho Kim, Republic of Korea
Yun Jin Kim , Malaysia
Yoshiyuki Kimura , Japan

Nebojša Kladar , Serbia
Mi Mi Ko , Republic of Korea
Toshiaki Kogure , Japan
Malcolm Koo , Taiwan
Yu-Hsiang Kuan , Taiwan
Robert Kubina , Poland
Chan-Yen Kuo , Taiwan
Kuang C. Lai , Taiwan
King Hei Stanley Lam, Hong Kong
Fanuel Lampiao, Malawi
Ilaria Lampronti , Italy
Mario Ledda , Italy
Harry Lee , China
Jeong-Sang Lee , Republic of Korea
Ju Ah Lee , Republic of Korea
Kyu Pil Lee , Republic of Korea
Namhun Lee , Republic of Korea
Sang Yeoup Lee , Republic of Korea
Ankita Leekha , USA
Christian Lehmann , Canada
George B. Lenon , Australia
Marco Leonti, Italy
Hua Li , China
Min Li , China
Xing Li , China
Xuqi Li , China
Yi-Rong Li , Taiwan
Vuanghao Lim , Malaysia
Bi-Fong Lin, Taiwan
Ho Lin , Taiwan
Shuibin Lin, China
Kuo-Tong Liou , Taiwan
I-Min Liu, Taiwan
Suhuan Liu , China
Xiaosong Liu , Australia
Yujun Liu , China
Emilio Lizarraga , Argentina
Monica Loizzo , Italy
Nguyen Phuoc Long, Republic of Korea
Zaira López, Mexico
Chunhua Lu , China
Ângelo Luís , Portugal
Anderson Luiz-Ferreira , Brazil
Ivan Luzardo Luzardo-Ocampo, Mexico

Michel Mansur Machado , Brazil
Filippo Maggi , Italy
Juraj Majtan , Slovakia
Toshiaki Makino , Japan
Nicola Malafrente, Italy
Giuseppe Malfa , Italy
Francesca Mancianti , Italy
Carmen Mannucci , Italy
Juan M. Manzanque , Spain
Fatima Martel , Portugal
Carlos H. G. Martins , Brazil
Maulidiani Maulidiani, Malaysia
Andrea Maxia , Italy
Avijit Mazumder , India
Isac Medeiros , Brazil
Ahmed Mediani , Malaysia
Lewis Mehl-Madrona, USA
Ayikoé Guy Mensah-Nyagan , France
Oliver Micke , Germany
Maria G. Miguel , Portugal
Luigi Milella , Italy
Roberto Miniero , Italy
Letteria Minutoli, Italy
Prashant Modi , India
Daniel Kam-Wah Mok, Hong Kong
Changjong Moon , Republic of Korea
Albert Moraska, USA
Mark Moss , United Kingdom
Yoshiharu Motoo , Japan
Yoshiki Mukudai , Japan
Sakthivel Muniyan , USA
Saima Muzammil , Pakistan
Benoit Banga N'guessan , Ghana
Massimo Nabissi , Italy
Siddavaram Nagini, India
Takao Namiki , Japan
Srinivas Nammi , Australia
Krishnadas Nandakumar , India
Vitaly Napadow , USA
Edoardo Napoli , Italy
Jorddy Neves Cruz , Brazil
Marcello Nicoletti , Italy
Eliud Nyaga Mwaniki Njagi , Kenya
Cristina Nogueira , Brazil

Sakineh Kazemi Noureini , Iran
Rômulo Dias Novaes, Brazil
Martin Offenbaecher , Germany
Oluwafemi Adeleke Ojo , Nigeria
Olufunmiso Olusola Olajuyigbe , Nigeria
Luís Flávio Oliveira, Brazil
Mozaniel Oliveira , Brazil
Atolani Olubunmi , Nigeria
Abimbola Peter Oluyori , Nigeria
Timothy Omara, Austria
Chiagoziem Anariochi Otuechere , Nigeria
Sokcheon Pak , Australia
Antônio Palumbo Jr, Brazil
Zongfu Pan , China
Siyaram Pandey , Canada
Niranjan Parajuli , Nepal
Gunhyuk Park , Republic of Korea
Wansu Park , Republic of Korea
Rodolfo Parreira , Brazil
Mohammad Mahdi Parvizi , Iran
Luiz Felipe Passero , Brazil
Mitesh Patel, India
Claudia Helena Pellizzon , Brazil
Cheng Peng, Australia
Weijun Peng , China
Sonia Piacente, Italy
Andrea Pieroni , Italy
Haifa Qiao , USA
Cláudia Quintino Rocha , Brazil
DANIELA RUSSO , Italy
Muralidharan Arumugam Ramachandran,
Singapore
Manzoor Rather , India
Miguel Rebollo-Hernanz , Spain
Gauhar Rehman, Pakistan
Daniela Rigano , Italy
José L. Rios, Spain
Francisca Rius Diaz, Spain
Eliana Rodrigues , Brazil
Maan Bahadur Rokaya , Czech Republic
Mariangela Rondanelli , Italy
Antonietta Rossi , Italy
Mi Heon Ryu , Republic of Korea
Bashar Saad , Palestinian Authority
Sabi Saheed, South Africa

Mohamed Z.M. Salem , Egypt
Avni Sali, Australia
Andreas Sandner-Kiesling, Austria
Manel Santafe , Spain
José Roberto Santin , Brazil
Tadaaki Satou , Japan
Roland Schoop, Switzerland
Sindy Seara-Paz, Spain
Veronique Seidel , United Kingdom
Vijayakumar Sekar , China
Terry Selfe , USA
Arham Shabbir , Pakistan
Suzana Shahar, Malaysia
Wen-Bin Shang , China
Xiaofei Shang , China
Ali Sharif , Pakistan
Karen J. Sherman , USA
San-Jun Shi , China
Insop Shim , Republic of Korea
Maria Im Hee Shin, China
Yukihiro Shoyama, Japan
Morry Silberstein , Australia
Samuel Martins Silvestre , Portugal
Preet Amol Singh, India
Rajeev K Singla , China
Kuttulebbai N. S. Sirajudeen , Malaysia
Slim Smaoui , Tunisia
Eun Jung Sohn , Republic of Korea
Maxim A. Solovchuk , Taiwan
Young-Jin Son , Republic of Korea
Chengwu Song , China
Vanessa Steenkamp , South Africa
Annarita Stringaro , Italy
Keiichiro Sugimoto , Japan
Valeria Sulsen , Argentina
Zewei Sun , China
Sharifah S. Syed Alwi , United Kingdom
Orazio Tagliatalata-Scafati , Italy
Takashi Takeda , Japan
Gianluca Tamagno , Ireland
Hongxun Tao, China
Jun-Yan Tao , China
Lay Kek Teh , Malaysia
Norman Temple , Canada

Kamani H. Tennekoon , Sri Lanka
Seong Lin Teoh, Malaysia
Menaka Thounaojam , USA
Jinhui Tian, China
Zipora Tietel, Israel
Loren Toussaint , USA
Riaz Ullah , Saudi Arabia
Philip F. Uzor , Nigeria
Luca Vanella , Italy
Antonio Vassallo , Italy
Cristian Vergallo, Italy
Miguel Vilas-Boas , Portugal
Aristo Vojdani , USA
Yun WANG , China
QIBIAO WU , Macau
Abraham Wall-Medrano , Mexico
Chong-Zhi Wang , USA
Guang-Jun Wang , China
Jinan Wang , China
Qi-Rui Wang , China
Ru-Feng Wang , China
Shu-Ming Wang , USA
Ting-Yu Wang , China
Xue-Rui Wang , China
Youhua Wang , China
Kenji Watanabe , Japan
Jintanaporn Wattanathorn , Thailand
Silvia Wein , Germany
Katarzyna Winska , Poland
Sok Kuan Wong , Malaysia
Christopher Worsnop, Australia
Jih-Huah Wu , Taiwan
Sijin Wu , China
Xian Wu, USA
Zuoqi Xiao , China
Rafael M. Ximenes , Brazil
Guoqiang Xing , USA
JiaTuo Xu , China
Mei Xue , China
Yong-Bo Xue , China
Haruki Yamada , Japan
Nobuo Yamaguchi, Japan
Junqing Yang, China
Longfei Yang , China

Mingxiao Yang , Hong Kong
Qin Yang , China
Wei-Hsiung Yang, USA
Swee Keong Yeap , Malaysia
Albert S. Yeung , USA
Ebrahim M. Yimer , Ethiopia
Yoke Keong Yong , Malaysia
Fadia S. Youssef , Egypt
Zhilong Yu, Canada
RONGJIE ZHAO , China
Sultan Zahiruddin , USA
Armando Zarrelli , Italy
Xiaobin Zeng , China
Y Zeng , China
Fangbo Zhang , China
Jianliang Zhang , China
Jiu-Liang Zhang , China
Mingbo Zhang , China
Jing Zhao , China
Zhangfeng Zhong , Macau
Guoqi Zhu , China
Yan Zhu , USA
Suzanna M. Zick , USA
Stephane Zingue , Cameroon

Contents

The Hydroalcoholic Extract of *Uncaria tomentosa* (Cat's Claw) Inhibits the Infection of Severe Acute Respiratory Syndrome Coronavirus 2 (SARS-CoV-2) *In Vitro*

Andres F. Yepes-Perez , Oscar Herrera-Calderón , Cristian A. Oliveros , Lizdany Flórez-Álvarez ,
María I. Zapata-Cardona , Lina Yepes , Wbeimar Aguilar-Jimenez , María T. Rugeles , and
Wildeman Zapata 

Research Article (11 pages), Article ID 6679761, Volume 2021 (2021)

Investigating Potential Inhibitory Effect of *Uncaria tomentosa* (Cat's Claw) against the Main Protease 3CL^{pro} of SARS-CoV-2 by Molecular Modeling

Andres F. Yepes-Pérez , Oscar Herrera-Calderon , José-Emilio Sánchez-Aparicio , Laura Tiessler-Sala , Jean-Didier Maréchal , and Wilson Cardona-G 

Research Article (14 pages), Article ID 4932572, Volume 2020 (2020)

Research Article

The Hydroalcoholic Extract of *Uncaria tomentosa* (Cat's Claw) Inhibits the Infection of Severe Acute Respiratory Syndrome Coronavirus 2 (SARS-CoV-2) *In Vitro*

Andres F. Yepes-Perez ¹, Oscar Herrera-Calderón ², Cristian A. Oliveros ³,
Lizdany Flórez-Álvarez ⁴, María I. Zapata-Cardona ⁴, Lina Yepes ⁴,
Wbeimar Aguilar-Jimenez ⁴, María T. Rugeles ⁴ and Wildeman Zapata ^{4,5}

¹Chemistry of Colombian Plants, Institute of Chemistry, Faculty of Exact and Natural Sciences, University of Antioquia-UdeA, Calle 70 No. 52-21, A.A 1226, Medellín, Colombia

²Academic Department of Pharmacology, Bromatology and Toxicology, Faculty of Pharmacy and Biochemistry, Universidad Nacional Mayor de San Marcos, Jr Puno 1002, Lima 15001, Peru

³Biomolecules Research Center, CIBIMOL, Universidad Industrial de Santander, UIS, Carrera 27 Calle 9, Bucaramanga, Colombia

⁴Grupo Inmunovirología, Facultad de Medicina, Universidad de Antioquia UdeA, Medellín, Colombia

⁵Grupo Infettare, Facultad de Medicina, Universidad Cooperativa de Colombia, Medellín, Colombia

Correspondence should be addressed to Oscar Herrera-Calderón; oherreraca@unmsm.edu.pe

Received 26 November 2020; Revised 11 January 2021; Accepted 2 February 2021; Published 24 February 2021

Academic Editor: Zheng Fei Ma

Copyright © 2021 Andres F. Yepes-Perez et al. This is an open access article distributed under the Creative Commons Attribution License, which permits unrestricted use, distribution, and reproduction in any medium, provided the original work is properly cited.

The coronavirus disease 2019 (COVID-19) has become a serious problem for public health since it was identified in the province of Wuhan (China) and spread around the world producing high mortality rates and economic losses. Nowadays, the WHO recognizes traditional, complementary, and alternative medicine for treating COVID-19 symptoms. Therefore, we investigated the antiviral potential of the hydroalcoholic extract of *Uncaria tomentosa* stem bark from Peru against SARS-CoV-2 *in vitro*. The antiviral activity of *U. tomentosa* against SARS-CoV-2 *in vitro* was assessed in Vero E6 cells using cytopathic effect (CPE) and plaque reduction assay. After 48 h of treatment, *U. tomentosa* showed an inhibition of 92.7% of SARS-CoV-2 at 25.0 µg/mL ($p < 0.0001$) by plaque reduction assay on Vero E6 cells. In addition, *U. tomentosa* induced a reduction of 98.6% ($p = 0.02$) and 92.7% ($p = 0.03$) in the CPE caused by SARS-CoV-2 on Vero E6 cells at 25 µg/mL and 12.5 µg/mL, respectively. The EC50 calculated for the *U. tomentosa* extract by plaque reduction assay was 6.6 µg/mL (4.89–8.85 µg/mL) for a selectivity index of 4.1. The EC50 calculated for the *U. tomentosa* extract by TCID50 assay was 2.57 µg/mL (1.05–3.75 µg/mL) for a selectivity index of 10.54. These results showed that *U. tomentosa*, known as cat's claw, has an antiviral effect against SARS-CoV-2, which was observed as a reduction in the viral titer and CPE after 48 h of treatment on Vero E6 cells. Therefore, we hypothesized that *U. tomentosa* stem bark could be promising in the development of new therapeutic strategies against SARS-CoV-2.

1. Introduction

The severe acute respiratory syndrome coronavirus 2 (SARS-CoV-2) has caused serious public health problems since it was identified in Wuhan (China) in late 2019 [1]. The World Health Organization (WHO) declared coronavirus disease

2019 (COVID-19) a pandemic on March 11, 2020 [2]. According to the latest report of the WHO, there have been 88,383,771 confirmed cases of COVID-19, including 1,919,126 deaths, as of 10 January 2021 [3]. When the novel coronavirus (SARS-CoV-2) arrived in Latin America, Brazil was the first South American country to declare a patient

with COVID-19 whereas Venezuela and Uruguay were the ultimate nations to confirm their patient zero, considering the pandemic epicenter after Europe [4]. Even though some vaccines have already been approved only with phase 3 results, currently, there is no preventive treatment or antiviral drug available against SARS-CoV-2 [5].

Nowadays, the World Health Organization (WHO) recognizes that traditional, complementary, and alternative medicine has many benefits [6]. Several candidates with possible antiviral effects have been explored from medicinal plants in the preclinical phase. *Uncaria tomentosa* (Willd.) DC. (*U. tomentosa*) belongs to the Rubiaceae family, which is also known as cat's claw and contains more than 50 phytochemicals [7]. Oxindole alkaloids (pentacyclic oxindole alkaloids (POA) and tetracyclic oxindole alkaloids (TOA)) have been recognized as a fingerprint of this species in some pharmacopeias, and several pharmacological activities are linked to this kind of alkaloids [8, 9]. It has been demonstrated that *U. tomentosa* exerts an antiviral effect on human monocytes infected with dengue virus 2 (DENV-2) [10] and herpes simplex virus type 1 (HSV-1) [11]. In our previous studies *in silico*, *U. tomentosa*'s components inhibited the SARS-CoV-2 enzyme 3CLpro and disrupted the interface of the receptor-binding domain of angiotensin-converting enzyme 2 (RBD-ACE-2) as well as the SARS-CoV-2 spike glycoprotein [12, 13]. Additionally, bioactivities such as anti-inflammatory [14], antiplatelet [15], and immunomodulatory [16] were reported in the literature. Furthermore, other components isolated from the stem bark such as quinovic acids, polyphenols (flavonoids, proanthocyanidins, and tannins), triterpenes, glycosides, and saponins were identified by instrumental methods [9, 17–20].

The evaluation of natural compounds to inhibit SARS-CoV-2 in preclinical studies might lead to discovering new antiviral drugs and to a better understanding of the viral life cycle [21]. Several cell lines such as human airway epithelial cells, Vero E6 cells, Caco-2 cells, Calu-3 cells, HEK293T cells, and Huh7 cells are considered the best models *in vitro* to determine the antiviral activity against SARS-CoV-2 [22]. Vero E6 cells highly express the ACE-2 receptor; they produce a high titer of viral particles and do not produce interferon [22]. Therefore, *in vitro* test in this cell line constitutes the first step at the beginning of the antiviral studies.

Although the pathophysiology of COVID-19 is not completely understood, a severe inflammatory process has been associated with the severity and progression of the disease [23]. Therefore, the immune activation so far described during the course of the infection as well as the pulmonary injury could be ameliorated by *U. tomentosa* linked to its traditional use as an anti-inflammatory in the folk medicine from South America for years [24].

Based on its antiviral activity on other ARN viruses and our *in silico* findings against SARS-CoV-2, we assayed the hydroalcoholic extract of *U. tomentosa* stem bark from Peru as a potential antiviral agent *in vitro* against this severe acute respiratory syndrome coronavirus 2.

2. Material and Method

2.1. Plant Material. *U. tomentosa* (cat's claw) used in this investigation is dispensed to patients of the Medicine Complementary Service of EsSalud (Social Health Insurance) in Peru for inflammatory disorders. The raw material (stem bark) of *U. tomentosa* was sourced from the Pharmacy Office of EsSalud in Ica, Peru. Next, the sample was transported to the Faculty of Medicine of the Universidad Nacional Mayor de San Marcos (UNMSM, Lima, Peru), in order to obtain the hydroalcoholic extract.

2.2. Obtaining Extract from Plant Material. One hundred grams of the raw plant material (stem bark) of *U. tomentosa* was powdered and extracted with 700 ml of 70% ethanol at room temperature for 7 days. Then, the extract was evaporated by using rotary evaporation to obtain a desiccated extract, which was stored at 4°C until further use.

2.3. Identification of the *U. tomentosa* Stem Bark Constituents by LC/MS (UHPLC-ESI+ -HRMS-Orbitrap). The identification of the main phytochemicals present within the hydroalcoholic extract of *U. tomentosa* was carried out on an LC Dionex UltiMate 3000 (Thermo Scientific, Germering, Germany) equipped with a degassing unit, a gradient binary pump, an autosampler with 120-vial well-plate trays, and a thermostatically controlled column compartment. The autosampler was held at 10°C, and the column compartment was maintained at 40°C. Chromatographic separation was performed on a Hypersil GOLD aQ column (Thermo Scientific, Sunnyvale, CA, USA; 100 mm × 2.1 mm id, 1.9 μm particle size) with an LC guard-column Accucore aQ Defender cartridge (Thermo Scientific, San Diego, CA, USA; 10 × 2.1 mm id, 2.6 μm particle size). The flow rate of the mobile phase containing ammonium formate (FA)/water (A) and FA/acetonitrile (B) was 300 μL/min. The initial gradient condition was 100% A, changed linearly to 100% B in 8 min, maintained for 4 min, returned to 100% A in 1 min, and maintained for 3 min. The injection volume was 1 μL. The LC was connected to an Exactive Plus Orbitrap mass spectrometer (Thermo Scientific, Bremen, Germany) with a heated electrospray ionization (HESI-II) source operated in the positive ion mode. The Vspray was evaluated at 1.5, 2.5, 3.5, and 4.5 kV. The nebulizer temperature was set at 350°C; the capillary temperature was 320°C; sheath gas and auxiliary gas (N₂) were adjusted to 40 and 10 arbitrary units, respectively. Nitrogen (>99%) was obtained from a generator (NM32LA, Peak Scientific, Scotland, UK). During the full scan MS, the Orbitrap-MS mass resolution was set at 70000 (full-width-at-half-maximum, at *m/z* 200, RFWHM) with an automatic gain control (AGC) target of 3 × 10⁶, a C-trap maximum injection time of 200 ms, and a scan range of *m/z* of 100–1000. The ions injected to the HCD cell via the C-trap were fragmented with stepped normalized collision energies of 20, 30, 40, and 50 eV. The mass spectra were recorded in the AIF (all-ion fragmentation) mode for each collision energy at an RFWHM of 35000, an AGC target of 3 × 10⁶, a

C-trap injection time of 50 ms, and a mass range of m/z of 80–1000. Full instrument calibration was performed every week using a Pierce LTQ Velos ESI Positive Ion Calibration Solution (Thermo Scientific, Rockford, IL, USA). The data obtained were analyzed using Thermo Xcalibur 3.1 software (Thermo Scientific, San Jose, CA, USA).

2.4. Preparation of Stock Solution of *U. tomentosa* Extract. One milligram of *U. tomentosa* hydroalcoholic extract was suspended in 1 mL of DMSO. The solution was maintained at room temperature, protected from light until use. To prepare a working solution, the stock was diluted to 50 mg/mL in DMEM supplemented with 2% fetal bovine serum (FBS) (5% final concentration DMSO).

2.5. Cell Lines and Virus. Vero E6 epithelial cell line from *Cercopithecus aethiops* kidney was donated by Instituto Nacional de Salud (INS) (Bogotá, Colombia). Cells were maintained in Dulbecco's modified Eagle's medium (DMEM) supplemented with 2% FBS and 1% penicillin-streptomycin. Cultures were maintained at 37°C, with 5% CO₂. Infections were done with a viral stock produced from a Colombian isolate of SARS-CoV-2 (hCoV-19/Colombia/ANT-UdeA-200325-01/2020) [25].

2.6. Cell Viability Assays. The viability of Vero E6 cells in the presence of the *U. tomentosa* extract was evaluated using an MTT (4,5-dimethylthiazol-2-yl)-2,5-diphenyl tetrazolium bromide) assay. Briefly, Vero E6 cells were seeded at a cell density of 1.0×10^4 cells/well in 96-well plates and incubated for 24 h at 37°C in a humidified 5% CO₂ atmosphere. Then, 100 µL of serial dilutions (1:2) of the *U. tomentosa* extract ranging from 3.1 to 50 µg/mL was added to each well and incubated for 48 h at 37°C with 5% CO₂. After incubation, the supernatants were removed, cells were washed twice with phosphate-buffered saline (PBS) (Lonza, Rockland, ME, USA), and 30 µL of the MTT reagent (Sigma-Aldrich) (2 mg/mL) was added. The plates were incubated for 2 hours at 37°C with 5% CO₂, protected from light. Then, formazan crystals were dissolved by adding 100 µL of pure DMSO to each well. Plates were read using a Multiskan GO spectrophotometer (Thermo) at 570 nm. The average absorbance of cells without treatment was considered as 100% of viability. Based on this control, the cell viability of each treated well was calculated. The treatment concentration with 50% cytotoxicity (the 50% cytotoxic concentration, CC50) was obtained by performing nonlinear regression followed by the construction of a concentration-response curve (GraphPad Prism). For the MTT assay, 2 independent experiments with four replicates of each experiment were performed ($n = 8$).

2.7. Antiviral Assay. The antiviral activity of the *U. tomentosa* extract against SARS-CoV-2 was evaluated with a pre-post strategy where the treatment was added before and after the infection. Briefly, Vero E6 cells were seeded at a density of 1.0×10^4 cells/well in 96-well plates and incubated for 24 h at 37°C with 5% CO₂. After

incubation, 50 µL of double dilutions of cat's claw (3.1–25 µg/mL) was added to the cell monolayers for 1 h at 37°C with 5% CO₂. Then, the treatment was removed, and cells were infected with SARS-CoV-2 stock at a multiplicity of infection (MOI) of 0.01 in 50 µL of DMEM supplemented with 2% FBS. The inoculum was removed 1 hour postinfection (h.p.i), replaced by 170 µL of cat's claw dilutions, and incubated for 48 h at 37°C with 5% CO₂. Then, cell culture supernatants were harvested and stored at –80°C for virus titration by plaque assay and TCID50 assay. The supernatant of infected cells without treatment was used as infection control. Chloroquine (CQ) at 50 µM was used as a positive control for antiviral activity; 2 independent experiments with 3 replicates of each experiment were performed ($n = 6$).

2.7.1. Plaque Assay for SARS-CoV-2 Quantification. The capacity of the *U. tomentosa* extract to decrease the PFU/mL of SARS-CoV-2 was evaluated by plaque assay on Vero E6 cells. Briefly, 1.0×10^5 Vero E6 cells per well were seeded in 24-well plates for 24 h at 37°C with 5% CO₂. Tenfold serial dilutions of the supernatants obtained from the antiviral assay (200 µL per well) were added by duplicate on cell monolayers. After incubation for 1 h at 37°C with 5% CO₂, the viral inoculum was removed and 1 mL of semisolid medium (1.5% carboxymethyl cellulose in DMEM 1X with 2% FBS and 1% penicillin-streptomycin) was added to each well. Cells were incubated for 5 days at 37°C with 5% CO₂. Then, cells were washed twice with PBS. Then, cells were fixed and stained with 500 µL of 4% formaldehyde/1% crystal violet solution for 30 minutes and washed with PBS. Plaques obtained from each condition were counted. The reduction in the viral titer after treatment with each concentration of the *U. tomentosa* extract compared to the infection control is expressed as inhibition percentage. Two independent experiments with two replicates of each experiment were performed ($n = 4$).

2.7.2. TCID50 Assay for SARS-CoV-2 Quantification. The capacity of the *U. tomentosa* extract to diminish the CPE caused by SARS-CoV-2 on Vero E6 cells was evaluated by TCID50 assay. Briefly, 1.2×10^4 Vero E6 cells per well were seeded in 96-well plates for 24 h at 37°C with 5% CO₂. Tenfold serial dilutions of the supernatants obtained from the antiviral assay (50 µL per well) were added by quadruplicate on cell monolayers. After 1 h incubation, at 37°C with 5% CO₂, the viral inoculum was removed and replaced by 170 µL of DMEM supplemented with 2% FBS. Cells were incubated for 5 days at 37°C with 5% CO₂. Then, cells were washed twice with PBS and then fixed and stained with 100 µL/well of 4% formaldehyde/1% crystal violet solution for 30 minutes. Cell monolayers were washed with PBS. The number of wells positive for CPE was determined for each dilution (CPE is considered positive when more than 30% of cell monolayer is compromised).

The viral titer of TCID50/mL was calculated based on the Spearman–Kärber method. The reduction of viral titer after treatment with each concentration of the *U. tomentosa* extract compared to infection control is expressed as

inhibition percentage. A control of cells without infection and treatment was included. Two independent experiments with two replicates of each experiment were performed ($n = 4$).

2.8. Statistical Analysis. The median inhibitory concentration (IC₅₀) values represent the concentration of the *U. tomentosa* extract that reduces virus particle production by 50%. The CC₅₀ values represent the cat's claw solution concentration that causes 50% cytotoxicity. The corresponding dose-response curves were fitted by nonlinear regression analysis using a sigmoidal model. The calculated selectivity index (SI) represents the ratio of CC₅₀ to IC₅₀. All data were analyzed with GraphPad Prism (La Jolla, CA, USA), and data are presented as mean \pm SEM. Statistical differences were evaluated via Student's *t*-test or Mann-Whitney *U* test; a value of $p \leq 0.05$ was considered significant, with * $p \leq 0.05$, ** $p \leq 0.01$, and *** $p \leq 0.001$.

3. Results

3.1. Identification of Components in the Hydroalcoholic Extract of *U. tomentosa* by LC/MS (UHPLC-ESI+ -HRMS-Orbitrap). Different constituents in the *U. tomentosa* stem bark such as spirooxindole alkaloids, indole glycoside alkaloids, quinovic acid glycosides, and proanthocyanidins were identified by LC-MS analysis (Table 1 and Supplementary materials S1–S6). The LC-MS data provided information on spirooxindole alkaloids as a broad peak that appeared at a retention time (t_R) of 4.82 min and showed an (M+H)⁺ ion at m/z 369.18018 that are characteristics for speciophylline, isopteropodine, isomitraphylline, uncarine F, mitraphylline, and pteropodine. Furthermore, two peaks at 4.99 and 5.18 min, respectively, showed the [M+H]⁺ ion at m/z 385.21127 that were identified as those isomeric spirooxindole-related alkaloids rhynchophylline and isorhynchophylline. On the other side, a molecular ion peak (M+H)⁺ of 547.22992 m/z , which eluted at 4.03 min, provided the identity of the indole glycoside alkaloid 3-dihydrocadambine. As expected, LC/MS phytochemical analysis showed that the hydroalcoholic extract of *U. tomentosa* was comprised predominantly of five proanthocyanidins (PAs), including proanthocyanidin C1, epiafzelechin-4 β -8, proanthocyanidin B2, epicatechin, and chlorogenic acid, which eluted at 3.76–4.25 min. Finally, LC-MS data along with ESI mass spectra gave characteristic protonated quasimolecular ions of isomeric quinovic acid glycosides ([M+H]⁺ ion at m/z 957.50458). In sum, LC/MS allowed the identification of known components in the hydroalcoholic extract of *U. tomentosa* used, such as alkaloids, quinovic acid glycosides, and proanthocyanidins (PAs), which play important roles in the biological activities of this medicinal herb and are considered as a fingerprint for quality control that ensures fitness for therapeutic uses.

3.2. The Cell Viability Assay on Vero E6 Cells in the Presence of the *U. tomentosa* Extract. The viability of Vero E6 cells in the presence of *U. tomentosa* was higher than 90.0% at

concentrations of 25.0 μ g/mL or lower, after 48 h of incubation (Figure 1). Cell viability at 50.0 μ g/mL was 17.3%; for this reason, this concentration was not included in the antiviral assay. The CC₅₀ calculated for *U. tomentosa* was 27.1 μ g/mL. Chloroquine at 50 μ M (positive control of inhibition) did not affect the viability of Vero E6 cells (Figure 1).

3.3. The *U. tomentosa* Extract Inhibited the Number of Infectious Viral Particles of SARS-CoV-2. An inhibition of 92.7% of SARS-CoV-2 was obtained after the treatment with *U. tomentosa* at 25.0 μ g/mL ($p < 0.0001$) by plaque reduction assay (Figure 2). The *U. tomentosa* extract also showed an inhibition of 31.4% and 34.9% of SARS-CoV-2 at 12.5 and 6.3 μ g/mL, respectively (Figure 2). An increase of 76.0% of PFU/mL of SARS-CoV-2 was obtained after the treatment with the *U. tomentosa* extract at 3.1 μ g/mL ($p = 0.02$) (Figure 2). The EC₅₀ calculated for the extract by plaque assay was 6.6 μ g/mL (4.89–8.85 μ g/mL) for a selectivity index of 4.1. Chloroquine (inhibition positive control) showed an inhibition of 100% of SARS-CoV-2 at 50 μ M ($p < 0.0001$) (Figure 2).

3.4. The *U. tomentosa* Extract Reduced the CPE of SARS-CoV-2. The *U. tomentosa* extract induced a reduction of 98.6% ($p = 0.02$), 92.7% ($p = 0.03$), 63.2%, and 60.4% in the CPE caused by SARS-CoV-2 on Vero E6 cells at 25, 12.5, 6.3, and 3.1 μ g/mL, respectively (Figure 3). The EC₅₀ calculated for the *U. tomentosa* extract by TCID₅₀ assay was 2.57 μ g/mL (1.05–3.75 μ g/mL) for a selectivity index of 10.54. Chloroquine showed an inhibition of 100% in the CPE of SARS-CoV-2 on Vero E6 cells at 50 μ M ($p = 0.008$) (Figure 3).

4. Discussion

In South America, the second wave of novel coronaviruses might be more aggressive, increasing the mortality rate and new cases [26]. Medical trials are underway to determine the efficacy of several vaccines against SARS-CoV-2 [27]. Otherwise, herbal medicines could become a promising option to tackle the ongoing pandemic caused by COVID-19 [28]. Some plant extracts and phytochemicals were modeled over numerous targets of SARS-CoV-2 by using *in silico* studies, which is the first step in the discovery of new drugs [29]. In China, the use of herbal formulas has been included in the protocol of primary attention in COVID-19 and medical trials were carried out, and promising results to ameliorate the symptoms were reported [30].

Our previous study of *U. tomentosa* (cat's claw) on this novel coronavirus using *in silico* analysis showed that two possible mechanisms could be involved in the *in vitro* antiviral activity against SARS-CoV-2. These findings revealed that 3CLpro, an essential enzyme for viral replication [31], showed key molecular interactions with speciophylline, cadambine, and proanthocyanidin B2, with high binding affinities ranging from -8.1 to -9.2 kcal/mol. [12]. On the other hand, phytochemicals of *U. tomentosa* such as proanthocyanidin C1, QAG-2, uncarine F, 3-

TABLE 1: LC/MS phytochemical analysis of the hydroalcoholic extract of *U. tomentosa*.

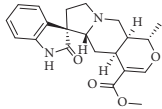
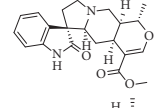
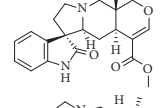
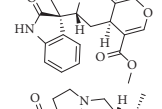
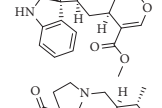
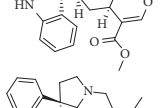
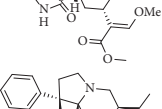
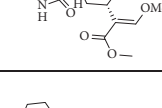
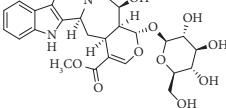
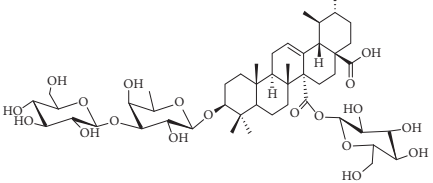
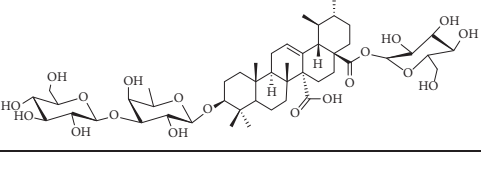
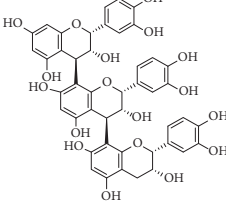
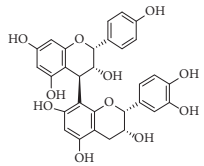
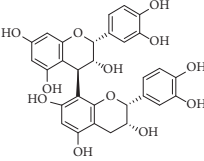
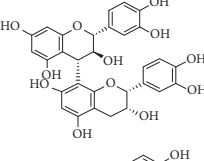
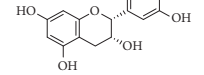
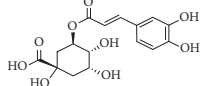
Peak	Compounds of cat's claw	t_R (min)	m/z (M + H) ⁺	Molecular formula	Chemical structure
Spirooxindole alkaloids					
1	Speciophylline	4.82	369.18018	C ₂₁ H ₂₄ N ₂ O ₄	
1	Isopteropodine	4.82	369.18018	C ₂₁ H ₂₄ N ₂ O ₄	
1	Isomitraphylline	4.82	369.18018	C ₂₁ H ₂₄ N ₂ O ₄	
1	Uncarine F	4.82	369.18018	C ₂₁ H ₂₄ N ₂ O ₄	
1	Mitraphylline	4.82	369.18018	C ₂₁ H ₂₄ N ₂ O ₄	
1	Pteropodine	4.82	369.18018	C ₂₁ H ₂₄ N ₂ O ₄	
2	Rhynchophylline	4.99	385.21127	C ₂₂ H ₂₈ N ₂ O ₄	
3	Isorhynchophylline	5.19	385.21140	C ₂₂ H ₂₈ N ₂ O ₄	
Indole glycoside alkaloids					
3	3-Dihydrocadambine	4.03	547.22992	C ₂₇ H ₃₄ N ₂ O ₁₀	
Quinovic acid glycosides					
4	QAG-1	4.84	957.50458	C ₄₈ H ₇₇ O ₁₉	
4	QAG-2	4.84	957.50458	C ₄₈ H ₇₇ O ₁₉	
Proanthocyanidins					
5	Proanthocyanidin C1	4.17	867.21191	C ₄₅ H ₃₈ O ₁₈	

TABLE 1: Continued.

Peak	Compounds of cat's claw	t_R (min)	m/z (M + H) ⁺	Molecular formula	Chemical structure
6	Epiafzelechin-4 β -8	4.25	563.15460	C ₃₀ H ₂₆ O ₁₁	
7	Proanthocyanidin B2	4.01	579.15002	C ₃₀ H ₂₆ O ₁₂	
7	Proanthocyanidin B4	4.01	579.15002	C ₃₀ H ₂₆ O ₁₂	
8	Epicatechin	4.15	291.08588	C ₁₅ H ₁₄ O ₆	
9	Chlorogenic acid	3.95	355.10220	C ₁₆ H ₁₈ O ₉	

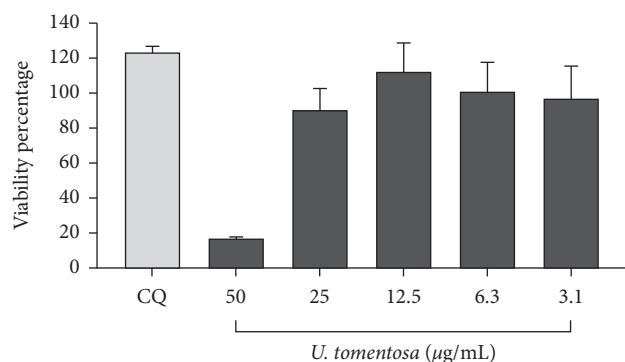


FIGURE 1: Viability of Vero E6 cells in the presence of the *U. tomentosa* extract. The figure represents the viability percentage of Vero E6 cells after 48 h of treatment with *U. tomentosa* (3.1 to 50.0 µg/mL). The viability percentages of treated cells were calculated based on the average absorbance control of cells without treatment. Chloroquine (CQ) was used as an inhibition control of the antiviral strategy. Bars represent mean values \pm SEM (2 independent experiments with four replicates of each experiment were performed, $n = 8$).

isodihydrocadambine, and uncaric acid (docking scores: -8.6 , -8.2 , -7.1 , -7.6 , and -7.0 kcal/mol, respectively) showed high binding affinity for the interface of the RBD-ACE-2. In addition, 3-dihydrocadambine, proanthocyanidin B4, proanthocyanidin B2, and proanthocyanidin C1 (-7.1 , -7.2 , -7.2 , and -7.0 kcal/mol, respectively) had the highest binding score on SARS-CoV-2 spike glycoprotein [13]. Since Vero E6 cells are commonly used to replicate SARS-CoV-2 due to the high expression level of the ACE-2

receptor and lack the ability to produce interferon [32], phytochemicals are the appropriate substrate to explore the antiviral activity of phytochemicals targeting the receptor binding as well as the SARS-CoV-2 main protease, which is a high-profile antiviral drug target, and several compounds have been discovered as main protease inhibitors [33, 34].

Mechanisms of the antiviral activity of the hydroalcoholic extract of *U. tomentosa*, on other viruses like Dengue (DEN-2), have been elucidated; alkaloids (pentacyclic alkaloids) from *U. tomentosa* induced apoptosis of infected cells and reduced inflammatory mediators such as TNF- α and IFN- α with similar effects to dexamethasone [10]. The quinovic acids (33.1–60 µg/mL) inhibited the vesicular stomatitis virus (VSV) [35], and the total extract at concentrations less than 15.75 µg/mL inhibited the herpes simplex virus (HSV-1) replication when added to Vero cells at the same time compared to the virus [11].

Here, we demonstrated that *U. tomentosa* also has an antiviral activity *in vitro* against the SARS-CoV-2 by inhibiting the release of infectious particles and reducing the cytopathic effect on Vero E6 cells. The EC50 was calculated at 6.6 µg/mL (95% CI: 4.89–8.85 µg/mL) by plaque assay and at 2.57 µg/mL (95% CI: 1.05–3.75 µg/mL) by TCID50 assay, whilst the CC50 was 27.1 µg/mL. In other medicinal plants assayed against SARS-CoV-2, similar antiviral activity was shown; in particular, Echinaforce® (an *Echinacea purpurea* preparation) exhibited an antiviral activity at 50 µg/mL [36]. Liu Shen capsule, a traditional Chinese medicine, inhibited the SARS-CoV-2 replication with an EC50 value of 0.6024 µg/mL and CC50 of 4.930 µg/mL [37]. Likewise, phyllirin (KD-1), a representative constituent of *Forsythia*

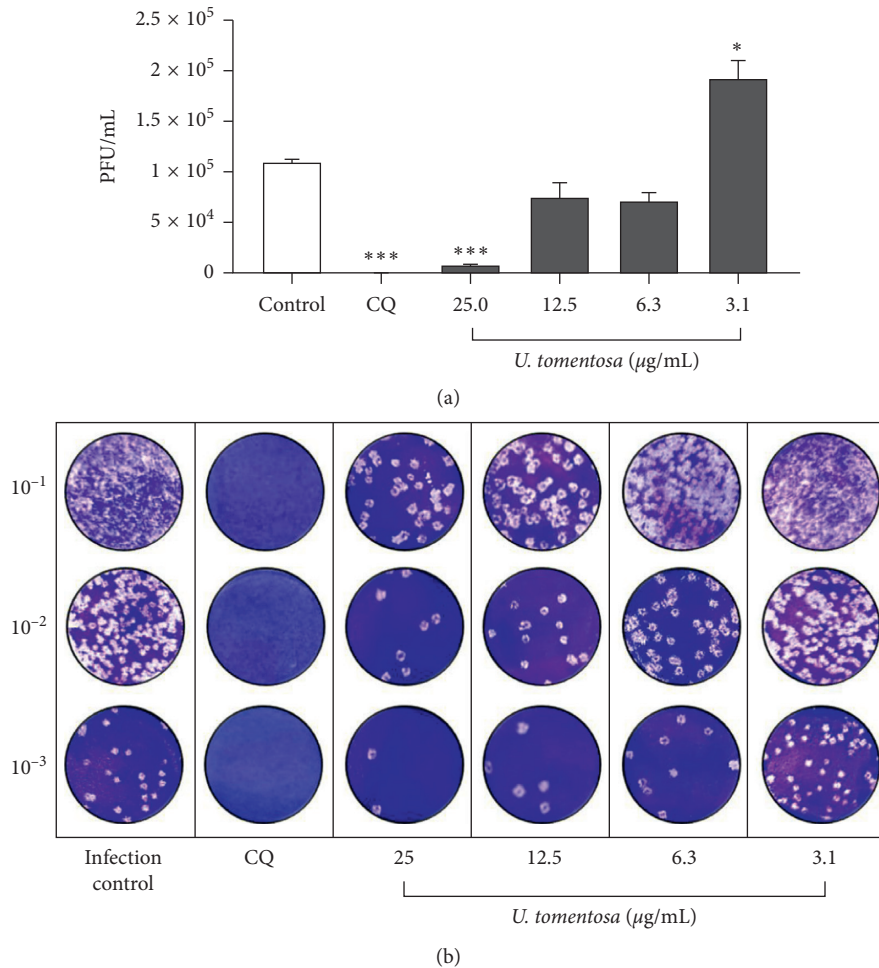


FIGURE 2: Antiviral activity *in vitro* of the *U. tomentosa* extract against SARS-CoV-2 by plaque assay. (a) The figure represents the viral titer (PFU/mL) of supernatants harvested after the treatment with the *U. tomentosa* extract quantified by plaque assay ($n = 4$). Chloroquine (CQ) was used as an inhibition positive control of the antiviral strategy. * $p \leq 0.05$, ** $p \leq 0.01$, and *** $p \leq 0.001$ (b) Representative plaques of the antiviral evaluation of the *U. tomentosa* extract against SARS-CoV-2 on Vero E6 cells.

suspensa (Thunb.), presented an EC₅₀ at 63.90 µg/mL and CC₅₀ of 1959 µg/mL [38]. Sulfated polysaccharides named RPI-27 and heparin inhibited SARS-CoV-2 *in vitro* with an EC₅₀ of 8.3 ± 4.6 µg/mL and 36 ± 14 µg/mL, respectively [39]. In our study, selectivity indices of 4.1 and 10.5 were obtained by plaque assay and TCID₅₀, respectively. According to a previous report [40], these results were classified as low selectivity ($SI \geq 2.0$ and < 5) and high selectivity ($SI \geq 10$), respectively. In spite of SI having a low value, theoretically having a higher value would be more effective and safer during *in vivo* treatment for a given viral infection. However, there is no evidence of severe toxicity of *U. tomentosa*, and traditionally, its popular use in the form of maceration or decoction is safe [41].

The lower concentration used of the *U. tomentosa* extract (3.1 µg/mL) caused a significant increase in the number of infectious viral particles compared to the infection control (Figure 2). This result could be due to compounds present in the extract that at this concentration promote an increase in cell proliferation or regulation of metabolic pathways that regulate the expression of viral receptors or synthesis of

proteins necessary for the viral replicative cycle [42, 43]. These findings demonstrate the importance of evaluating and identifying the compounds present in *U. tomentosa* with antiviral effect against SARS-CoV-2 and selecting the proper concentration for use.

There is enough evidence that *U. tomentosa* could ameliorate a wide array of symptoms associated with COVID-19, like the severe inflammation characterized by a cytokine storm [24] causing endothelial dysfunction. According to the antiviral activity of *U. tomentosa* against SARS-CoV-2, several biochemical mechanisms could be involved in each phase of the viral life cycle. As previously reported in our *in silico* studies, *U. tomentosa* could interfere with viral entrance into host cells [12], affecting viral replication [13]. Furthermore, ACE-2 receptors, which are expressed in Vero E6 cells, could also be blocked by the phytochemicals of *U. tomentosa* during the entrance of SARS-CoV-2 into the host cells, and the aforementioned studies backed up our hypothesis [13].

Besides, it might control the hyperinflammation, via inhibition of IL-1 α , IL-1 β , IL-17, and TNF- α [44], reduce

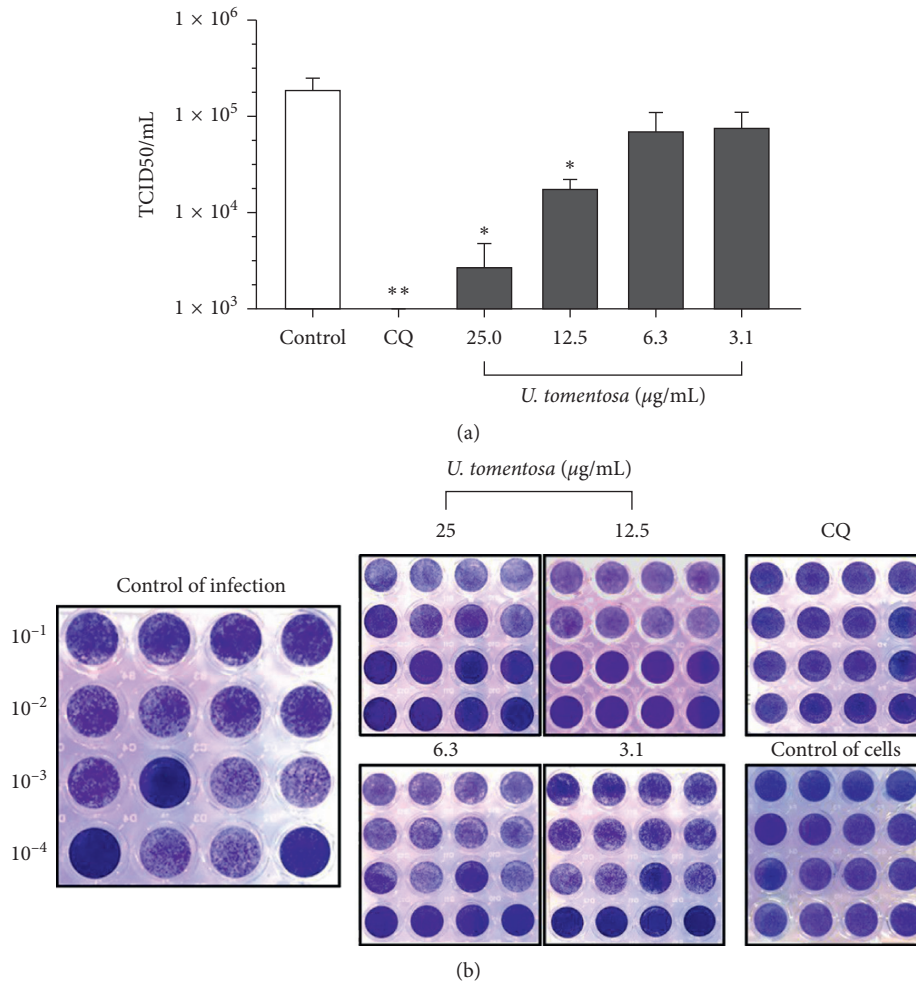


FIGURE 3: Antiviral activity *in vitro* of the *U. tomentosa* extract against SARS-CoV-2 by TCID50 assay. (a) The figure represents the viral titer (TCID50/mL) quantified by TCID50 assay on supernatants harvested from the treatment with the *U. tomentosa* extract ($n = 4$). Chloroquine (CQ) was used as an inhibition positive control of the antiviral strategy. * $p \leq 0.05$ and ** $p \leq 0.01$. (b) Representative images of the antiviral evaluation of the *U. tomentosa* extract against SARS-CoV-2 on Vero E6 cells by TCID50 assay revealed by crystal violet.

oxidative stress [45], and protect the endothelial barrier, via inhibition of IL-8, which is linked to the induction of permeability [46]. It also has antithrombotic potential via antiplatelet mechanism and by thrombin inhibition [15]. Furthermore, *U. tomentosa* modulates the immune system by extending lymphocyte survival via an antiapoptotic mechanism [47]. It is known that the 3 α protein of severe acute respiratory syndrome-associated coronavirus induces apoptosis in Vero E6 cells [48]; therefore, the phytochemicals found in the hydroalcoholic extract could inhibit this process and protect against the inflammatory cascade. Interestingly, *U. tomentosa* bark extract reduced the lung inflammation produced by ozone in mice [49].

Based on our results, *U. tomentosa* is a promising medicinal herb to combat COVID-19, but it is necessary to continue with animal models followed by clinical trials to validate our results in the context of COVID-19 patients. This study is the first approach to evaluate the potential use of *U. tomentosa* against SARS-CoV-2; we have to explore specific mechanisms of inhibition and propose the main

molecules involved with the antiviral activity. As shown in our phytochemical analysis, the presence of chemical groups determined by LC/MS (UHPLC-ESI + -HRMS-Orbitrap), such as spirooxindole alkaloids, indole glycoside alkaloids, quinovic acid glycosides, and proanthocyanidins, suggests that they could be responsible for the described activity. Here, the mechanisms discussed about the hydroalcoholic extract of *U. tomentosa* are only inferred under the mechanisms evaluated in other RNA viruses reported in the literature and also our previous *in silico* studies on SARS-CoV-2.

In regard to the antiviral activity of *U. tomentosa*, the EC50 was calculated at 6.6 $\mu\text{g/mL}$, which is an indicator of a promising activity as an extract, but it cannot be taken as a reference value to reach plasma concentration because *U. tomentosa* extract presented several phytochemicals, which were not quantified and individually tested. Since cat's claw has been used in clinic for other diseases, there are no clinical studies carried out and reported pharmacokinetic data. However, in mice, the administration of 5 mg/Kg per

oral of six Uncaria alkaloids presented a bioavailability ranging between 27.3% and 68.9% and with a maximum plasma concentration (C_{max}) between 305.3 ± 68.8 ng/mL and 524.5 ± 124.5 ng/mL [50].

Additionally, the recommended dose of *U. tomentosa* is one gram given two to three times daily [51]. A standardized extract consisting of less than 0.5% oxindole alkaloids and 8% to 10% carboxy alkyl esters has been used at doses of 250 to 300 mg in clinical studies [52]. In humans, no toxic symptoms were reported with a usual administration of 350 mg/day for 6 weeks [53, 54] and 300 mg dry extract daily for 12 weeks [55]. Traditional uses such as tinctures, decoctions, capsules, extracts, and teas are prepared and, in a decoction, up to 20 g of raw bark per liter of water has been used; although this information is based on traditional practices, this equates to 4 mg oxindole alkaloids [56]. Thus, we hypothesized that the antiviral activity on SARS-CoV-2 is attributed to the whole extract synergized by all its phytochemicals acting by different mechanisms discussed above.

5. Conclusion

U. tomentosa has been widely used as an anti-inflammatory and immunomodulatory agent. Previous studies have shown that *U. tomentosa* has a broad spectrum of effects on several RNA viruses. In this study, we demonstrated that hydroalcoholic extract of *U. tomentosa* stem bark inhibited the release of SARS-CoV-2 infectious particles and reduced the cytopathic effect caused by the virus on Vero E6 cell line, underlying the importance of continuing this investigation with specific *in vitro* assays, followed by studies in animal models, and finally validating its use in clinical trials. Our investigation shows for the first time the antiviral effect of *U. tomentosa* on this novel coronavirus (SARS-CoV-2).

Data Availability

All data used to support the findings of this study can be made available from the corresponding author upon request.

Disclosure

This manuscript was initially submitted as a preprint, which is available at <https://www.biorxiv.org/content/10.1101/2020.11.09.372201v1.full>.

Conflicts of Interest

The authors declare that they have no known conflicts of interest or personal relationships that could have appeared to influence the work reported in this paper.

Acknowledgments

The authors would like to thank Prof. Dr. Elena E. Stashenko, Biomolecules Research Center, CIBIMOL, Universidad Industrial de Santander (UIS), for providing the phytochemical analysis of the plant studied in the present study. This study was financed by Universidad de Antioquia

and Universidad Cooperativa de Colombia (BPIN 2020000100131-SGR).

Supplementary Materials

S1: 2D structures for the major bioactive constituents of *U. tomentosa*. S2: LC-MS data for spirooxindole alkaloids: speciophylline, isopteropodine, isomitraphylline, uncarine F, mitraphylline, and pteropodine. S3: LC-MS data for spirooxindole alkaloids: rhynchophylline and isorynchophylline. S4: LC-MS data for indole glycoside alkaloids: 3-dihydrocadambine. S5: LC-MS data for quinovic acid glycosides: QAG-1 and QAG-2. S6: LC-MS data for proanthocyanidins: proanthocyanidin C1, epiafzelechin-4 β -8, proanthocyanidin B2/B4, epicatechin, and chlorogenic acid. (*Supplementary Materials*)

References

- [1] J. Harcourt, A. Tamin, X. Lu et al., "Severe acute respiratory syndrome coronavirus 2 from patient with coronavirus disease, United States," *Emerging Infectious Diseases*, vol. 26, no. 6, pp. 1266–1273, 2020.
- [2] Y. Takeda, T. Murata, D. Jamsransuren et al., "Saxifraga spinulosa-derived components rapidly inactivate multiple viruses including SARS-CoV-2," *Viruses*, vol. 12, no. 7, 699 pages, 2020.
- [3] World Health Organization (WHO), World Health Organization, "WHO coronavirus disease (COVID-19) dashboard," 2020, <https://covid19.who.int>.
- [4] J. A. Poterico and O. Mestanza, "Genetic variants and source of introduction of SARS-CoV-2 in South America," *Journal of Medical Virology*, vol. 92, no. 10, 2020.
- [5] C.-C. Lai, T.-P. Shih, W.-C. Ko, H.-J. Tang, and P.-R. Hsueh, "Severe acute respiratory syndrome coronavirus 2 (SARS-CoV-2) and coronavirus disease-2019 (COVID-19): the epidemic and the challenges," *International Journal of Antimicrobial Agents*, vol. 55, no. 3, Article ID 105924, 2020.
- [6] WHO, "WHO supports scientifically-proven traditional medicine no title," 2020, <https://www.afro.who.int/news/who-supports-scientificallly-proven-traditional-medicine>.
- [7] L. Z. De Oliveira, I. L. G. Farias, M. L. Rigo et al., "Effect of Uncaria tomentosa extract on apoptosis triggered by oxaliplatin exposure on HT29 cells," *Evidence-Based Complementary and Alternative Medicine*, vol. 2014, Article ID 274786, 10 pages, 2014.
- [8] M. E. Heitzman, C. C. Neto, E. Winiarz, A. J. Vaisberg, and G. B. Hammond, "Ethnobotany, phytochemistry and pharmacology of uncaria (Rubiaceae)," *Phytochemistry*, vol. 66, no. 1, pp. 5–29, 2005.
- [9] O. Lock, E. Perez, M. Villar, D. Flores, and R. Rojas, "Bioactive compounds from plants used in peruvian traditional medicine," *Natural Product Communications*, vol. 11, no. 3, pp. 315–337, 2016.
- [10] S. R. I. N. Reis, L. M. M. Valente, A. L. Sampaio et al., "Immunomodulating and antiviral activities of uncaria tomentosa on human monocytes infected with dengue virus-2," *International Immunopharmacology*, vol. 8, no. 3, pp. 468–476, 2008.
- [11] T. Caon, S. Kaiser, C. Feltrin et al., "Antimutagenic and antiherpetic activities of different preparations from uncaria tomentosa (cat's claw)," *Food and Chemical Toxicology*, vol. 66, pp. 30–35, 2014.

- [12] A. F. Yepes-Pérez, O. Herrera-Calderon, J.-E. Sánchez-Aparicio et al., "Investigating potential inhibitory effect of *Uncaria tomentosa* (cat's claw) against the main protease 3CLpro of SARS-CoV-2 by molecular modeling," *Evidence-Based Complementary and Alternative Medicine*, vol. 2020, pp. 1–14, 2020.
- [13] A. F. Yepes-Pérez, O. Herrera-Calderon, and J. Quintero-Saumeth, "Uncaria tomentosa (cat's claw): a promising herbal medicine against SARS-CoV-2/ACE-2 junction and SARS-CoV-2 spike protein based on molecular modeling," *Journal of Biomolecular Structure and Dynamics*, vol. 117 pages, 2020.
- [14] M. Sandoval-Chacón, J. H. Thompson, X. J. Zhang et al., "Antiinflammatory actions of cat's claw: the role of NF- κ B," *Alimentary Pharmacology & Therapeutics*, vol. 12, no. 12, pp. 1279–1289, 1998.
- [15] J. Kolodziejczyk-Czepas, M. Ponczek, M. Sady-Janczak, R. Pilarski, and B. Bukowska, "Extracts from *Uncaria tomentosa* as antiplatelet agents and thrombin inhibitors –the *in vitro* and *in silico* study," *Journal of Ethnopharmacology*, vol. 267, Article ID 113494, 2020.
- [16] R. M. Lenzi, L. H. Campestrini, L. M. Okumura et al., "Effects of aqueous fractions of *uncaria tomentosa* (Willd.) D.C. on macrophage modulatory activities," *Food Research International*, vol. 53, no. 2, pp. 767–779, 2013.
- [17] M. Navarro-Hoyos, R. Lebrón-Aguilar, J. E. Quintanilla-López et al., "Proanthocyanidin characterization and bioactivity of extracts from different parts of *uncaria tomentosa* L. (cat's claw)," *Antioxidants*, vol. 6, no. 1, 2017.
- [18] F. Dietrich, S. Kaiser, L. Rockenbach et al., "Quinovic acid glycosides purified fraction from *uncaria tomentosa* induces cell death by apoptosis in the T24 human bladder cancer cell line," *Food and Chemical Toxicology*, vol. 67, pp. 222–229, 2014.
- [19] R. Aquino, N. De Tommasi, F. De Simone, and C. Pizza, "Triterpenes and quinovic acid glycosides from *uncaria tomentosa*," *Phytochemistry*, vol. 45, no. 5, pp. 1035–1040, 1997.
- [20] E. M. C. Peñaloza, S. Kaiser, P. E. De Resende et al., "Chemical composition variability in the *uncaria tomentosa* (cat's claw) wild population," *Química Nova*, vol. 38, no. 3, pp. 378–386, 2015.
- [21] M. D. Sacco, C. Ma, P. Lagarias et al., "Structure and inhibition of the SARS-CoV-2 main protease reveals strategy for developing dual inhibitors against M pro and cathepsin L," *Science Advances*, vol. 6, no. 50, 2020.
- [22] K. Takayama, "Vitro and animal models for SARS-CoV-2 research," *Trends in Pharmacological Sciences*, vol. 41, no. 8, pp. 513–517, 2020.
- [23] M. K. Bohn, A. Hall, L. Sepiashvili et al., "Pathophysiology of COVID-19: mechanisms underlying disease severity and progression," *Physiology*, vol. 35, no. 5, 2020.
- [24] A. O. Ferreira, H. C. Polonini, and E. C. F. Dijkers, "Postulated adjuvant therapeutic strategies for COVID-19," *Journal of Personalized Medicine*, vol. 10, no. 3, p. 80, 2020.
- [25] F. J. Díaz, W. Aguilar-Jiménez, L. Flórez-Álvarez et al., "Aislamiento y caracterización de una cepa temprana de SARS-CoV-2 durante la epidemia de 2020 en Medellín, Colombia," *Biomedica*, vol. 40, no. 2, pp. 148–158, 2020.
- [26] S. Xu and Y. Li, "Beware of the second wave of COVID-19," *The Lancet*, vol. 395, pp. 1321–1322, Article ID 10233, 2020.
- [27] A. A. Rabaan, S. H. Al-Ahmed, R. Sah et al., "SARS-CoV-2/ COVID-19 and advances in developing potential therapeutics and vaccines to counter this emerging pandemic," *Annals of Clinical Microbiology and Antimicrobials*, vol. 19, no. 1, p. 40, 2020.
- [28] L. Ni, L. Zhou, M. Zhou, J. Zhao, and D. W. Wang, "Combination of western medicine and Chinese traditional patent medicine in treating a family case of COVID-19," *Frontiers of Medicine*, vol. 14, no. 2, pp. 210–214, 2020.
- [29] R. R. Narkhede, A. V. Pise, R. S. Cheke, and S. D. Shinde, "Recognition of natural products as potential inhibitors of COVID-19 main protease (Mpro): in-silico evidences," *Natural Products and Bioprospecting*, vol. 10, no. 5, pp. 297–306, 2020.
- [30] X. Xiong, P. Wang, K. Su, W. C. Cho, and Y. Xing, "Chinese herbal medicine for coronavirus disease 2019: a systematic review and meta-analysis," *Pharmacological Research*, vol. 160, Article ID 105056, 2020.
- [31] W. Dai, B. Zhang, X.-M. Jiang et al., "Structure-based design of antiviral drug candidates targeting the SARS-CoV-2 main protease," *Science*, vol. 368, no. 6497, pp. 1331–1335, 2020.
- [32] N. S. Ogando, T. J. Dalebout, J. C. Zevenhoven-Dobbe et al., "SARS-coronavirus-2 replication in vero E6 cells: replication kinetics, rapid adaptation and cytopathology," *Journal of General Virology*, vol. 101, no. 9, pp. 925–940, 2020.
- [33] L. Zhang, D. Lin, X. Sun et al., "Crystal structure of SARS-CoV-2 main protease provides a basis for design of improved α -ketoamide inhibitors," *Science*, vol. 368, no. 6489, pp. 409–412, Apr. 2020.
- [34] C. Ma, M. D. Sacco, B. Hurst et al., "Boceprevir, GC-376, and calpain inhibitors II, XII inhibit SARS-CoV-2 viral replication by targeting the viral main protease," *Cell Research*, vol. 30, no. 8, pp. 678–692, 2020.
- [35] R. Aquino, F. De Simone, C. Pizza, C. Conti, and M. L. Stein, "Plant metabolites. Structure and *in vitro* antiviral activity of quinovic acid glycosides from *uncaria tomentosa* and *guettarda platypoda*," *Journal of Natural Products*, vol. 61, no. 7, pp. 936–938, 1989.
- [36] J. Signer, H. R. Jonsdottir, W. C. Albrich et al., "In vitro virucidal activity of echinaforce®, an echinacea purpurea preparation, against coronaviruses, including common cold coronavirus 229E and SARS-CoV-2," *Virology Journal*, vol. 17, no. 1, 136 pages, 2020.
- [37] Q. Ma, W. Pan, R. Li et al., "Liu Shen capsule shows antiviral and anti-inflammatory abilities against novel coronavirus SARS-CoV-2 via suppression of NF- κ B signaling pathway," *Pharmacological Research*, vol. 158, Article ID 104850, 2020.
- [38] Q. Ma, R. Li, W. Pan et al., "Phillyrin (KD-1) exerts anti-viral and anti-inflammatory activities against novel coronavirus (SARS-CoV-2) and human coronavirus 229E (HCoV-229E) by suppressing the nuclear factor kappa B (NF- κ B) signaling pathway," *Phytomedicine*, vol. 78, Article ID 153296, 2020.
- [39] P. S. Kwon, H. Oh, S.-J. Kwon et al., "Sulfated polysaccharides effectively inhibit SARS-CoV-2 *in vitro*," *Cell Discovery*, vol. 6, no. 1, p. 50, 2020.
- [40] A. I. Trujillo-Correa, D. C. Quintero-Gil, F. Diaz-Castillo et al., "In vitro and *in silico* anti-dengue activity of compounds obtained from *psidium guajava* through bioprospecting," *BMC Complementary and Alternative Medicine*, vol. 19, no. 1, 298 pages, 2019.
- [41] T. Maruoka, A. Kitanaka, Y. Kubota et al., "Lemongrass essential oil and citral inhibit Src/Stat3 activity and suppress the proliferation/survival of small-cell lung cancer cells, alone or in combination with chemotherapeutic agents," *International Journal of Oncology*, vol. 1, pp. 1738–1748, 2018.
- [42] S. Wichit, R. Hamel, E. Bernard et al., "Imipramine inhibits chikungunya virus replication in human skin fibroblasts through interference with intracellular cholesterol trafficking," *Scientific Reports*, vol. 7, 3145 pages, 2017.

- [43] F. Tabatabaei, M. Moezizadeh, and F. Javand, "Effects of extracts of *Salvadora persica* on proliferation and viability of human dental pulp stem cells," *Journal of Conservative Dentistry: JCD*, vol. 18, no. 4, pp. 315–320, 2015.
- [44] R. Rojas-Duran, G. González-Aspajo, C. Ruiz-Martel et al., "Anti-inflammatory activity of mitraphylline isolated from *Uncaria tomentosa* bark," *Journal of Ethnopharmacology*, vol. 143, no. 3, pp. 801–804, 2012.
- [45] A. C. Cheng, C. B. Jian, Y. T. Huang et al., "Induction of apoptosis by *Uncaria tomentosa* through reactive oxygen species production, cytochrome c release, and caspases activation in human leukemia cells," *Food and Chemical Toxicology*, vol. 45, no. 11, pp. 2206–2218, 2007.
- [46] R. S. Lima-Junior, C. Da Silva Mello, C. F. Kubelka, A. C. Siani, and L. M. M. Valente, "*Uncaria tomentosa* alkaloidal fraction reduces paracellular permeability, il-8 and ns1 production on human microvascular endothelial cells infected with dengue virus," *Natural Product Communications*, vol. 8, no. 11, pp. 1547–1550, 2013.
- [47] M. Sandoval, R. M. Charbonnet, N. N. Okuhama et al., "Cat's claw inhibits TNF α production and scavenges free radicals: role in cytoprotection," *Free Radical Biology and Medicine*, vol. 29, no. 1, pp. 71–78, 2000.
- [48] P. T. W. Law, C. H. Wong, T. C. C. Au et al., "The 3a protein of severe acute respiratory syndrome-associated coronavirus induces apoptosis in vero E6 cells," *Journal of General Virology*, vol. 86, no. 7, pp. 1921–1930, 2005.
- [49] F. J. Cisneros, M. Jayo, and L. Niedziela, "An *Uncaria tomentosa* (cat's claw) extract protects mice against ozone-induced lung inflammation," *Journal of Ethnopharmacology*, vol. 96, no. 3, pp. 355–364, 2005.
- [50] L. Chen, J. Ma, X. Wang, and M. Zhang, "Simultaneous determination of six *Uncaria* alkaloids in mouse blood by UPLC-MS/MS and its application in pharmacokinetics and bioavailability," *BioMed Research International*, vol. 2020, Article ID 1030269, 11 pages, 2020.
- [51] G. E.-S. Batiha, A. Magdy Beshbishy, L. Wasef et al., "*Uncaria tomentosa* (Willd. ex Schult.) DC.: a review on chemical constituents and biological activities," *Applied Sciences*, vol. 10, no. 8, p. 2668, 2020.
- [52] Y. Sheng, "DNA repair enhancement of aqueous extracts of in a human volunteer study," *Phytomedicine*, vol. 8, no. 4, pp. 275–282, 2001.
- [53] L. G. Valerio and G. F. Gonzales, "Toxicological aspects of the South American herbs cat's claw (*Uncaria tomentosa*) and maca (*Lepidium meyenii*): a critical synopsis," *Toxicological Reviews*, vol. 24, no. 1, 11 pages, 2005.
- [54] L. C. L. De Paula, F. Fonseca, F. Perazzo et al., "*Uncaria tomentosa* (cat's claw) improves quality of life in patients with advanced solid tumors," *Journal of Alternative and Complementary Medicine*, vol. 21, no. 1, pp. 22–30, 2015.
- [55] M. R. C. Schetinger, I. L. G. Farias, M. C. S. Araújo et al., "*Uncaria tomentosa* for reducing side effects caused by chemotherapy in CRC patients: clinical trial," *Evidence-Based Complementary and Alternative Medicine*, vol. 2012, Article ID 892182, 8 pages, 2012.
- [56] K. Keplinger, G. Laus, M. Wurm, M. P. Dierich, and H. Teppner, "*Uncaria tomentosa* (Willd.) DC. - ethnomedicinal use and new pharmacological, toxicological and botanical results," *Journal of Ethnopharmacology*, vol. 64, no. 1, pp. 23–34, 1998.

Research Article

Investigating Potential Inhibitory Effect of *Uncaria tomentosa* (Cat's Claw) against the Main Protease 3CL^{Pro} of SARS-CoV-2 by Molecular Modeling

Andres F. Yepes-Pérez ¹, Oscar Herrera-Calderon ², José-Emilio Sánchez-Aparicio ³,
Laura Tiessler-Sala ³, Jean-Didier Maréchal ³, and Wilson Cardona-G ¹

¹Chemistry of Colombian Plants, Institute of Chemistry, Faculty of Exact and Natural Sciences, University of Antioquia-UdeA, Calle 70 No. 52-21, A.A 1226, Medellín, Colombia

²Academic Department of Pharmacology, Bromatology and Toxicology, Faculty of Pharmacy and Biochemistry, Universidad Nacional Mayor de San Marcos, Jr Puno 1002, Lima 15001, Peru

³Insilichem, Departament de Química, Universitat Autònoma de Barcelona, Edifici C.n., 08193 Cerdanyola del Vallés, Barcelona, Spain

Correspondence should be addressed to Andres F. Yepes-Pérez; andresf.yepes@udea.edu.co, Oscar Herrera-Calderon; oherreracalderon@gmail.com, and Jean-Didier Maréchal; jeandidier.marechal@uab.cat

Received 7 May 2020; Accepted 25 July 2020; Published 1 October 2020

Guest Editor: Zheng Feei Ma

Copyright © 2020 Andres F. Yepes-Pérez et al. This is an open access article distributed under the Creative Commons Attribution License, which permits unrestricted use, distribution, and reproduction in any medium, provided the original work is properly cited.

COVID-19 is a disease caused by severe acute respiratory syndrome coronavirus 2. Presently, there is no effective treatment for COVID-19. As part of the worldwide efforts to find efficient therapies and preventions, it has been reported the crystalline structure of the SARS-CoV-2 main protease M^{Pro} (also called 3CL^{Pro}) bound to a synthetic inhibitor, which represents a major druggable target. The druggability of M^{Pro} could be used for discovering drugs to treat COVID-19. A multilevel computational study was carried out to evaluate the potential antiviral properties of the components of the medicinal herb *Uncaria tomentosa* (Cat's claw), focusing on the inhibition of M^{Pro}. The *in silico* approach starts with protein-ligand docking of 26 Cat's claw key components, followed by ligand pathway calculations, molecular dynamics simulations, and MM-GBSA calculation of the free energy of binding for the best docked candidates. The structural bioinformatics approaches led to identification of three bioactive compounds of *Uncaria tomentosa* (speciophylline, cadambine, and proanthocyanidin B2) with potential therapeutic effects by strong interaction with 3CL^{Pro}. Additionally, *in silico* drug-likeness indices for these components were calculated and showed good predicted therapeutic profiles of these phytochemicals. Our findings suggest the potential effectiveness of Cat's claw as complementary and/or alternative medicine for COVID-19 treatment.

1. Introduction

Severe acute respiratory syndrome coronavirus 2 (SARS-CoV-2) is a part of coronavirus (CoV) family and was initially identified in Wuhan, China, at the end of December 2019. COVID-19 is highly contagious and is most frequently transmitted from human to human, spreading the virus easily to other countries in a very short time [1]. According to the last report of the World Health Organization (WHO), the severe acute respiratory syndrome (coronavirus disease

(COVID-19)) caused by SARS-CoV-2 is considered a pandemic, affecting Asia and Europe with the highest death rate followed by America and other regions, causing serious public health problems and considerable economic losses worldwide [2]. Respiratory viral infections are the frequent causes of morbidity and millions of hospital admissions in developing countries every year [3]. For this reason, the pharmacotherapy based on natural products may be a proper alternative for treating viral diseases. On the other hand, traditional medicine is practiced by native South

American inhabitants who know the medicinal properties of many plants from the rainforest [4]. Therefore, many of them are collected by ethnobotanists who investigate their resources as antimicrobial [5] and antitumor agents and being the main source for target selection during scientific investigation on compounds with antiviral activity [6]. The biodiversity of South America countries [7] offers a series of medicinal plants which could combat the symptoms of infections such as coronavirus disease COVID-19.

Uncaria tomentosa (Willd. ex Schult.) DC. named Cat's claw ("uña de gato" in Spanish) is a woody vine indigenous to the Peruvian Amazon and other tropical areas of South and Central America and belongs to Rubiaceae family [8]. In Peru, natives from the villages in the region of Chanchamayo and Nevati near Puerto Bermudez, Junin, boil approximately 20 g of sliced root bark in 1 liter of water for 45 min commonly and use it in religious purposes and curatives [9]. This species is marketed as dry and ground material remarkably in recent years, being widely studied in all aspects mainly by chemical (isolated chemical structures) and bioassays *in silico*, *in vitro*, *in vivo* and some medical trials. Currently, the raw material of *U. tomentosa* is dispensed in Public Hospitals of the Social Health Insurance (EsSalud-Peru) as Complementary Medicine Service (CMS) [10]. Traditionally, extracts prepared by root and bark decoction are used against several diseases, such as allergies, arthritis, inflammations, rheumatism infections, and cancer [11]. However, its popular use has been widely known worldwide, and analytical tests can be found in the United States Pharmacopeia and dosage forms have been authorized only as dietary supplements. Currently, there are about 34 species of *Uncaria*, with *Uncaria tomentosa* being the most common species [12].

Bioactive constituents of *U. tomentosa* extracts include proanthocyanidins (proanthocyanidin B2 or epicatechin- $(4\beta \rightarrow 8)$ -epicatechin, the main component; proanthocyanidin B4, proanthocyanidin C1, an epicatechin trimer, epiafzelechin- $4\beta \rightarrow 8$ -epicatechin, and an epicatechin tetramer) [13], oxindole alkaloids (isopteropodine, pteropodine, rhynchophylline, myrtraphylline, speciophylline, uncarine F, and uncarine E) [14], indole alkaloidal glucosides (cadambine, 3-dihydrocadambine, and 3-isodihydrocadambine) [15, 16], quinovic acid glycosides, tannins, polyphenols, catechins, beta-sitosterol, and proteins which individually or synergistically contribute to their therapeutic properties [8, 17–24].

In regard to the antiviral properties of *U. tomentosa*, the alkaloid fraction has been demonstrated to be the most effective on human monocytes infected with dengue virus-2 (DENV) *in vitro* [25]. Another study revealed that only the alkaloidal fraction has inhibitory activity on dengue virus, and the negative effect was observed with the nonalkaloidal fraction [26]. In another study, the antiherpetic activity of *U. tomentosa* seems to be associated with polyphenols or their synergistic effect with pentacyclic oxindole alkaloids or quinovic acid glycosides [27]. *U. tomentosa* hydroethanolic extracts demonstrated a significant *in vitro* inhibitory effect on the replication of herpes simplex virus type 1, and the inhibition of viral

attachment in the host cells was characterized as the main mechanism of its antiviral activity [27]. Furthermore, other investigations mentioned immunomodulating activity which includes stimulation of phagocytosis, enhancement of B- and T-lymphocytes, suppression of NF-kappa B, and enhancement of IL-1 and IL-6 [28, 29]. In a Peruvian study on rats, the investigators found that phagocytosis was increased and might act as the potent inhibitor of TNF- α [30]. In 2008, a study evidenced a possible drug-drug interaction between Cat's claw and protease inhibitors such as saquinavir, atazanavir, and ritonavir, increasing level of these drugs in plasma [31]. Individuals supplemented with a novel water-soluble extract of *Uncaria tomentosa* (C-Med-100®) showed increased effectiveness of pneumococcal vaccination as a result of an increase the lymphocyte/neutrophil ratios of peripheral blood and a reduced decay in the 12 serotype antibody titer responses to pneumococcal vaccination [32].

With neither drugs nor vaccines approved against SARS-CoV-2 yet, finding strategies to diminish the impact of the pandemic is fundamental. Medicinal herbs and, more particularly, those demonstrating antiviral activities are possible allies in this quest. Their use could slow down the spreading of the disease. Particularly in developing countries, in which the accessibility to these plants is easier and more economically viable, adding these medicinal herbs to the general medical kit may be beneficial. In addition, traditional knowledge of these remedies may reduce possible side effects, allowing them to be implemented with fewer medical risks [33].

On the basis of the aforementioned background of *Uncaria tomentosa* (Cat's claw), this work aims at computationally identifying potential bioactive compounds against COVID-19. It focuses on possible interactions and inhibition of the 3CL^{PRO} protease (also called M^{PRO}). 3CL^{PRO} is responsible for 100% of the proteolytic mechanism of the virus and is involved in virulence, infectivity, transcription, and replication cycle of the virus [34, 35]. It has been identified as the main druggable target of SARS-CoV-2 for new antiviral discovery. Moreover, its X-ray structure has been recently released, hence allowing possible computational analysis. In fact, several computational studies have already been undertaken on this system including a long 20 μ s molecular dynamics (MD) study and virtual screening of several databases [36, 37].

Here, our study stands on a multilevel computational strategy reminiscent to those applied at the early stage of current state-of-the-art drug discovery pipelines and includes (1) protein-ligand docking of all bioactive compounds of Cat's claw against 3CL^{PRO} structure, (2) simulations of the ligand pathway of the best predicted compounds from step 1 to evaluate the convenient entrance mechanism of the compounds to the binding site, (3) molecular dynamics simulation to assess the stability of the best protein-ligand complexes from step 2, (4) calculation of the free energy of binding based on MD postprocessing (MM-GBSA), and (5) calculation of pharmacokinetics parameters for the most qualified compounds resulting from the previous parts of the

protocol. The study leads to identification of at least three compounds with potential antiviral activity in Cat's claw-based products to propose the extract of *Uncaria tomentosa* as a rapid phytotherapeutic option for COVID-19.

2. Materials and Methods

2.1. Protein Structure and Setup. Calculated binding affinity of the main constituents of the Cat's claw extracts (Table 1) was explored against the main protease 3CL^{pro} of SARS-CoV-2 findings, a facile therapeutic option for anti-coronavirus therapy; the crystal structure of the protease 3CL^{pro} was downloaded from the Protein Data Bank (PDB entry code 6LU7) [38]; and all bounded ligands, ions, and solvent molecules were manually removed using the DS Visualizer 2.5 program. For docking studies, the structure of the selected protein was parameterized using AutoDock Tools [38]. Gasteiger partial charges were calculated, and polar hydrogens to facilitate the formation of hydrogen bonds were added.

2.2. Ligand Dataset Preparation and Optimization. Ligands used in this study are major components of the Cat's claw extracts, a potent irreversible inhibitor recently reported for COVID-19 virus 3CL^{pro} (namely, N3) [39], and three well-known FDA-approved viral protease inhibitors that may be repurposed to treat COVID-19 [40–46]. The 2D structures of 26 Cat's claw constituents were obtained as mol.2 files from the ZINC database [47]. The resultant compounds were submitted to MarvinSketch 8.3 [48] to correct the protonation states of the ligands at physiological pH 7.4 and its structures were parameterized using AutoDockTools to add full hydrogens to the ligands, to assign rotatable bonds, and to compute Gasteiger charges and save the resulting structure in the required format for use with AutoDock. All possible flexible torsions of the ligand molecules were defined using AUTOTORS in PDBAutoDockTools [49] to promote the calculated binding with the SARS-CoV-2 protease structure.

2.3. Docking-Based Virtual Screening. Our docking protocol was performed using AutoDock 4.2 with the Lamarckian genetic algorithm and default procedures to dock a flexible ligand to a rigid protein. Docking simulation was carried out on the main protease 3CL^{pro} of the SARS-CoV-2 cleavage site (PDB code: 6LU7), where the enzyme residues are in proximity to the recently reported potent inhibitor, known as N3, which was co-crystallized in complex with the main SARS-CoV-2 protease. Once a potential binding site was identified, 26 compounds which are the major components of the Cat's claw extracts were docked to this enzyme site to determine the most probable and the most energetically favorable binding conformations. To accomplish rigorous docking simulations involving a grid box to the identified catalytic site, Autodock Vina 1.1.2 was used [49]. The exhaustiveness was 20 for each protein-ligand pair (number of internal independent runs). The active site was surrounded by a docking grid of 42 Å³ with a grid spacing of 0.375 Å.

TABLE 1: Best binding energy (kcal/mol) based on AutoDock scoring of the main constituents of Cat's claw into the cleavage site of the novel SARS-CoV-2 main protease (PDB ID: 6LU7).

Main constituents of Cat's claw	Best binding energy (kcal/mol)
<i>Spiroindole alkaloids</i>	
Speciophylline	-8.1
Isopteropodine	-6.6
Isomitraphylline	-7.6
Uncarine F	-8.2
Mitraphylline	-7.0
Pteropodine	-7.0
Rhynchophylline	-5.9
Isorhynchophylline	-6.1
<i>Indole glycoside alkaloids</i>	
Cadambine	-8.6
3-Dihydrocadambine	-8.0
3-Isodihydrocadambine	-8.0
<i>Polyhydroxylated triterpenes</i>	
PHT-1	-6.8
Uncaric acid	-7.0
Floridic acid	-7.6
<i>Quinovic acid glycosides</i>	
QAG-1	-7.8
QAG-2	-7.4
QAG-3	-7.2
QAG-4	-7.9
QAG-5	-7.8
QAG-6	-7.8
<i>Proanthocyanidins</i>	
Chlorogenic acid	-6.8
Epicatechin	-7.2
Proanthocyanidin B2	-9.2
Epiarzelechin-4β-8-epicatechin	-8.9
Proanthocyanidin B4	-9.2
Proanthocyanidin C1	-8.8
<i>References</i>	
N3 ^a	-8.1 (-8.1) ^b , (-8.3) ^c , (-7.9) ^d
Remdesivir ^h	-8.5
Ritonavir ^h	-8.1 (-7.7) ^e , (-7.5) ^f , (-8.9) ^g
Lopinavir ^h	-8.0 (-8.4) ^e , (-7.4) ^f , (-9.4) ^g

^aPotent irreversible inhibitor of SARS-CoV-2 virus 3CL^{pro}. ^bBinding affinity reported by [47]. ^cBinding affinity reported by [77]. ^dBinding affinity reported by [78]. ^eBinding affinity reported by [79]. ^fBinding affinity reported by [80]. ^gBinding affinity reported by [3]. ^hFDA-approved antiviral drugs promising to treat SARS-CoV-2 [81–83].

Affinity scores (in kcal/mol) given by AutoDock Vina for all compounds were obtained and ranked based on the free energy binding theory (more negative value means greater binding affinity). The resulting structures and the binding docking poses were graphically inspected to check the interactions using DS Visualizer 2.5 (<http://3dsbiovia.com/products/>) or PyMOL Molecular Graphics System 2.0 programs [50].

2.4. GPathFinder Calculations. To assess the feasibility of the binding route for the ligand, ten runs of GPathFinder [51] calculations for each ligand-protease complex were performed. The ligand was placed at the position obtained from docking calculations and required to search for a possible

unbinding route outside the protease. Full flexibility was allowed for the ligand along the pathway including rotameric states of amino acid side chain and backbone motions based on some previous MD simulations of 10 μ s. A clustering was carried out by means of the quality threshold methodology [52] to obtain a pool of 110 representative frames from a 10 μ s simulation of the apo structure [53]. This pool of representative frames was used as the possible conformations that the protease could adopt during the ligand transport. Vina score and steric clashes were minimized to obtain a total of 120 solutions for each run. A complete input file to use with version 1.2.1 of the software is provided in Supplementary Materials (available here).

2.5. Molecular Dynamics Simulations. All the molecular dynamics (MD) simulations were carried out using the dimeric structure of the COVID main protease available in the PDB [53] (code 6lu7) as a receptor. The best-scored docking positions were used as starting conformations for the ligands. Two ligands (one for each monomer) were placed at symmetric positions of the dimeric structure. The protein was prepared by removing waters and crystallographic small molecules from the PDB structure to have the protease residues free of interaction with the ligands during the simulation. Finally, protons were then added through the algorithm implemented in UCSF Chimera Software [54].

MD simulations were set up with the LEaP, which was instructed to solvate the protein with a cubic box of pre-equilibrated TIP3P water molecules and balance the total charge with Na⁺ ions (ions94.lib library). The AMBER14SB force field [55] was used for the standard residues, while the GAFF force field was adopted for the remaining atoms. The geometries of the ligands were optimized in water solvent (SMD continuum model) at DFT level of theory using Gaussian09 [56]. Geometry and frequency calculations were performed using the B3LYP hybrid functional with 6-31G(d,p) as basis set and included Grimme's dispersion [57]. Atomic charges were computed using the RESP protocol (restrained electrostatic potential) at the same level of theory, and the atom types and force constants and equilibrium parameters were assigned using antechamber and parmchk2 from AmberTools18 [58].

For all the MDs, the solvent and the whole system were sequentially submitted to 3000 energy minimization steps to relax possible steric clashes. Then, thermalization of the system was achieved by increasing the temperature from 100 K up to 300 K. MD simulations under periodic boundary conditions were carried out for 250 ns with the OpenMM engine [59] using OMMProtocol [60]. Three simulations were run in total, considering the following protease-ligand systems: speciophylline, cadambine, and proanthocyanidin B2.

Analysis of the trajectories was carried out by means of CPPTraj implemented in AmberTools18. The MD trajectory was considered converged when a stable exploration of the conformational space was achieved. In particular, a stable conformation or a pool of relative stable conformations visited for a statistically consistent number of times were

considered as convergence indicators [47]. Considering the alpha carbons of the protease backbone, RMSD from the minimized structure, all-to-all frames RMSD, and cluster counting analysis were performed. Moreover, to ensure that dynamic transitions occur between different conformations, a principal component analysis (PCA) was carried out by plotting the two principal modes relative to each other.

The distance from the geometric center of the ligand to the center of the binding site was computed along all the trajectories. Alpha carbons of the residues GLY143, CYS145, HIS163, HIS164, GLU166, GLN189, and THR190 were considered to calculate the center of the binding site, and the distance from the crystallographic inhibitor N3 to that binding site center (3.947 Å) was taken as reference for comparison.

2.6. Prediction of Drug-Likeness Properties for the Most Docking Promissory Compounds. Drug-likeness prediction along with further ADME properties presents a wide range of opportunities for a rapid new antiviral drug discovery. The drug-like and ADME properties for the most active components of the Cat's claw extracts (constituents having the highest binding affinity) were screened using open-access cheminformatic platforms such as Molinspiration (for molecular weight (MW), rotatable bonds, and polar surface area (PSA) descriptors), ALOGPS 2.1 (for log $P_{o/w}$ descriptor), and Pre-ADMET 2.0 to predict four pharmaceutically relevant properties such as intestinal permeability (App. Caco-2), albumin-binding proteins (K_{HSA}), Madin-Darby Canine Kidney (MDCK Line) cell permeation, and intestinal absorption (%HIA). These parameters establish movement, permeability, absorption, and action of potential drugs [61–64]. The interpretation of both MDCK and Caco-2 permeability using PreADMET [65] is as follows:

- (1) Permeability lower than 25: low permeability
- (2) Permeability between 25 and 500: medium permeability
- (3) Permeability higher than 500: high permeability

3. Results and Discussion

3.1. Database of Cat's Claw Bioactive Compounds. This study was performed to identify if certain components of the Cat's claw extracts have potential therapeutic effects against COVID-19. To do so, a database of 26 compounds that have shown prevalence on the herbal therapeutic activity has been generated (Figure 1) [8, 9, 13, 23, 25, 29, 66–72]. Our initial hypothesis is that Cat's claw should contain molecules with highest therapeutic profiles against SARS-CoV-2, because of their interaction with 3CL^{PRO} main protease.

Currently, some of this chemical components have been isolated and synthesized, such as cadambine [73], speciophylline [74], and proanthocyanidin B2 [75], and several bioassays were performed for their derived products. However, pure drugs that are industrially produced or isolated from plants may be an option for their high biological activity, but they could have some disadvantages.

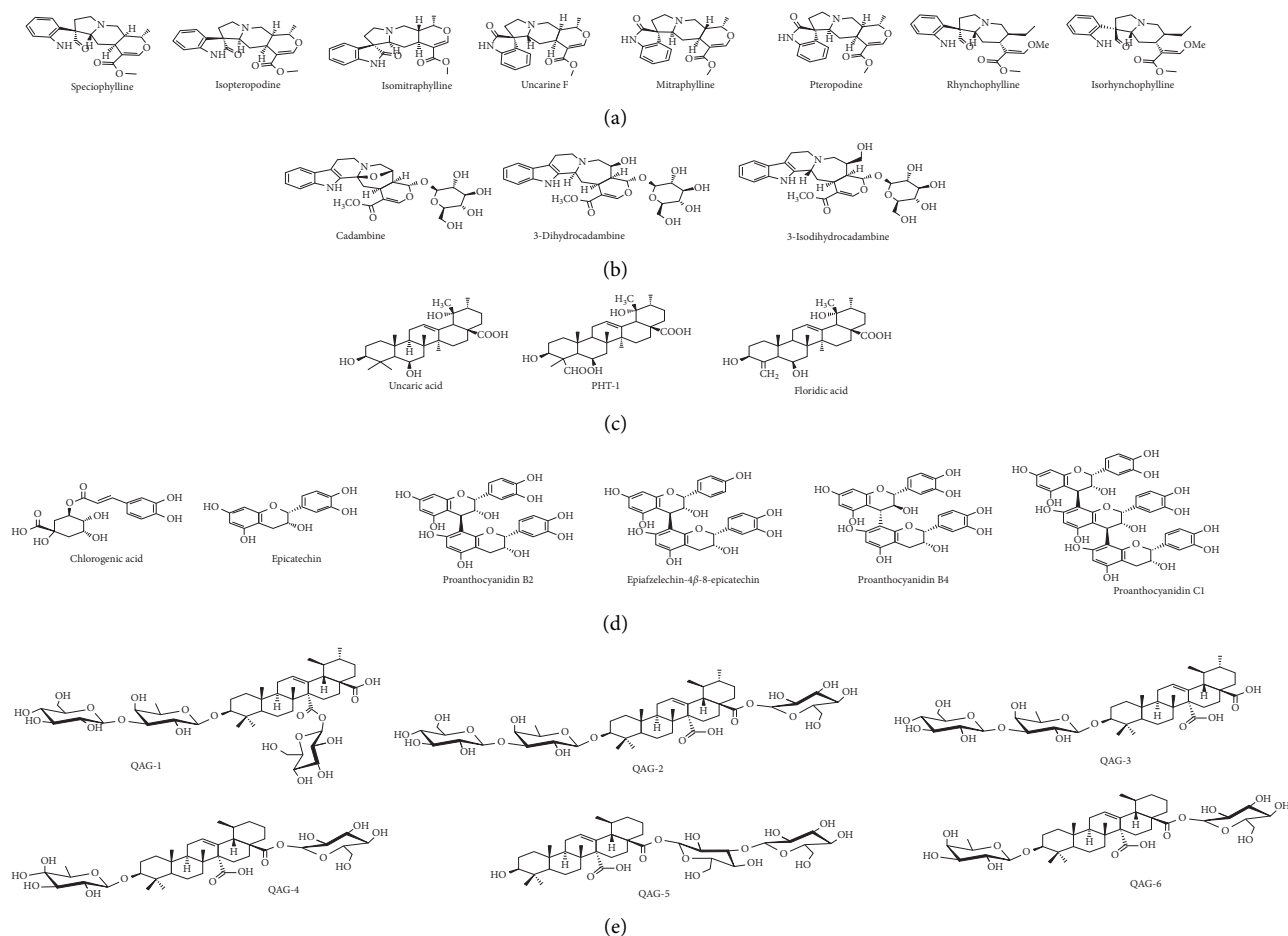


FIGURE 1: 2D structures for the major bioactive constituents of Cat's claw studied as ligands against the SARS-CoV-2 main protease. (a) Spiroindole alkaloids; (b) indole glycosides alkaloids; (c) polyhydroxylated triterpenes; (d) quinovic acid glycosides.

Pure drugs rarely have the same degree of activity as a total extract at comparable concentrations or doses of the active component [76]. This phenomenon is attributed to the absence of interacting substances present in the extract. Furthermore, many plants contain chemical constituents that could inhibit drug resistance in viral diseases. Synthesized drugs are often more expensive to produce, being unavailable to the poorest populations. In contrast, herbal medicines used as infusion, decoction, and maceration can sometimes be grown and produced locally, at lower cost, taking into account its ethnopharmacological use.

3.2. Docking Results. Despite limitations in terms of energetic functions (scoring) and conformational sampling (limited to ligand rotational bound mainly and restricted local motion of the protein at the most), protein-ligand dockings are still today the main computational strategy to identify potential binders to a given protein target. Protein-ligand dockings of the 26 constituents of Cat's claw were performed against the three-dimensional structure of the SARS-Cov-2 main protease 3CL^{Pro} (PDB: 6LU7) [37] to study the potential of ethanolic extracts of Cat's claw for COVID-19 treatment based on its majority of components.

The structure of 3CL^{Pro} shows the protein to be a homodimer with a subunit of 306 amino acids long (Figure 2). The catalytic site is mainly constituted by loops and hairpins that suggests a flexible site, a feature common in many proteases. The co-crystallized N3 drug stands in the catalytic site that defines the subsites of cleavage site S1 and is characterized by the following amino acids: THR190, GLN189, GLU166, HIS164, CYS145, GLY143, GLU166, HIS163, PHE140, ASN142, MET49, HIS41, MET165, ARG188, and ASP187.

This site was defined as the binding pocket for the docking runs. Because of the symmetry in the X-ray structure between the two dimers of 3CL^{Pro}, dockings were performed on only one monomer. Molecular docking studies were performed with Autodock for all compounds.

All compounds show docked structures that fit well into the S1 cavity of 3CL^{Pro} (Figures 3(a) and 3(b)) and with good predicted docking scores that range from -5.9 to -9.2 kcal/mol (Table 1 and Figure S1). In general, calculations revealed that most of the 12 amino acids involved in the N3-3CL^{Pro} interactions identified in the X-ray structures also constitute the binding pocket of the docking solutions. In particular, most predicted complexes have the interaction fingerprint with CYS145, GLU166, MET165, GLN189, and GLY143, the

glycoside ones. These findings are also consistent with previous reports demonstrating the antiviral properties of the alkaloid fractions from Cat's claw [25]. Amongst those compounds, speciophylline and cadambine are particularly interesting since they are part of the phytochemical fingerprint for *Uncaria tomentosa* (Cat's claw).

From this part of the study, nine components are computationally estimated to have similar or even better binding affinities for the 3CL^{Pro} cleavage site S1 than the current protease inhibitor N3 and other antiviral drugs. Speciophylline, cadambine, and proanthocyanidin B2 were selected for further investigation since they are the best representative of three different families of compounds of the Cat's claw fractions (docking scores of -8.1, -8.6, and -9.2 kcal/mol, respectively).

3.3. Ligand Pathway Analysis. A first series of refinements consisted in the simulation of the ligand pathways of speciophylline, cadambine, and proanthocyanidin B2 to the catalytic site S1 of 3CL^{Pro}. Indeed, protein-ligand docking does not account with the protein motions associated to the transition of the ligands from the solvent to the binding site, a phenomenon that could lead to false positives in screening steps of drug discovery processes and to avoid for further stages. To ascertain the accessibility of the compounds to the cleavage site, calculations were performed using the GPathFinder software [51]. For each compound, 120 channels were calculated (10 runs segmented in finding the 12 lowest energy paths), and their results were averaged. The sampling of the protein structure was based on 110 snapshots from the 10 μ s simulation of the unbound structure recently released [85], hence allowing that large-scale motions (domain motions) could be accounted in the simulation.

For the three compounds, the calculations tend to converge to the same entrance pathway that mainly involve rearrangements of the loop and hairpin motives that constitute the S1 cleavage site as well as some breathing motions involving the alpha helix domain of the dimer (Figure 4). For all ligands, low energy barriers are observed and none overcome the 5.3 kcal/mol in average (± 3.2 kcal/mol) (see Table S1). This value is consistent with the relatively solvent exposed binding site of the protease and suggests the absence of restrictive motions for the binding of the ligands. It was noticed that the lowest barrier is observed for speciophylline with a value of 2.4 kcal/mol.

To this point, our study shows that (1) speciophylline, cadambine, and proanthocyanidin B2 (epicatechin-(4 β -8)-epicatechin) have good predicted binding affinity for S1 cleavage site and (2) they can naturally access it without noticeable energetic cost.

3.4. Molecular Dynamics (MD) Simulations and Calculations of the Free Energy of Binding. With higher confidence on the viability of our docking predictions for speciophylline, cadambine, and proanthocyanidin B2, we further evaluated the stability of the docked complexes throughout molecular dynamics simulations. Calculations were performed with

openMM software [86] and the Amber force field [55] (for details, readers can refer to Section 2). It is important to notice that the simulations were carried out on the dimeric (hence complete) structure of the protease-ligand complexes after their reconstruction by symmetric operation. For each system, then the stoichiometry of ligand: protein is 2:1 (2 ligands for one dimer).

We assessed the quality of our MD experiment by using four different criteria: (1) root mean square deviation of the backbone (RMSD), (2) all-to-all RMSD, (3) principal component analysis (PCA), and (4) cluster counting. This combination of analytical tools has previously proven to be a reliable assessment methodology of protein structural convergence [87]. Moreover, ligand and protein flexibility were assessed by calculation of RMSF analysis. By taking all these parameters into account, all simulations were run until 250 ns each (see Figure 5 for speciophylline as an illustrative case of analysis, and ESI Figures S3 and S4 for cadambine and proanthocyanidin B2).

Based on the analysis of these different variables and visual inspection, a clear behavior appears along the molecular dynamics, which is summarized as follows:

- (1) The overall trajectories of all systems are stable with no modification in terms of the secondary structure. Only slight transitions on the tertiary structure (intra- and intermonomeric interfaces) are observed though of different magnitudes depending on which the Cat's claw component is bound and their motion during the course of the MD.
- (2) For speciophylline, both monomers behave in a very symmetric manner with the ligands remaining well sited into the cavity during the entire course of the simulation and at the same location of the initial docking solution (Figures 5(b) and 5(c)). However, two different orientations are observed. The orientation with higher time of residence is very close to the initial docked complex with most of the interactions of the cleavage site maintained through additional hydrogen bonds that appear with Gln189 and Gln192 (Figure 5(d), Table S2). The second one shows speciophylline displaying a slight rotation around its main axis of inertia (Figure 5(b)). This second orientation appears related to the loss of the hydrogen bond of the Gln189 as well as a slight rearrangement of the α domain with respect to the β domain. These changes in the ternary structure are also related to modifications of the interfaces between both monomers. It is to note that these motions are consistent with those observed for ligand binding simulation of the previous GPathFinder calculations (see Section 3.3 and Figure 4).
- (3) For cadambine and proanthocyanidin B2, the overall fold is also very stable. However, a conformational change occurs at about 200 ns, which essentially affects the tertiary and quaternary nature of the system (Figures S3 and S4). Further inspection shows that both monomers have also distinct behaviors.

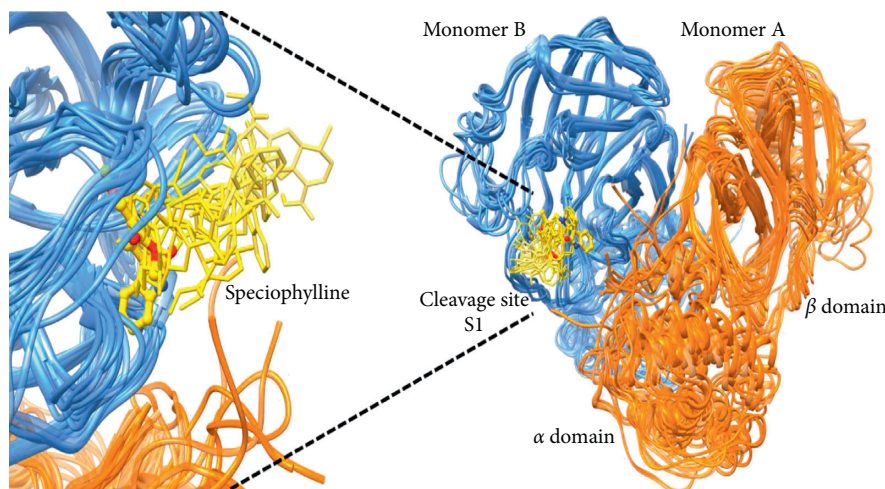


FIGURE 4: Schematic view of the entrance pathway for speciophylline into monomer B of the 3CL^{PRO} protease of SARS-CoV-2. The ligand is shown in yellow and the protein in orange (monomer A) and blue (monomer B). Snapshots of the lowest energy pathway are presented with the ligand represented in thin sticks and the final pose in ball and stick.

While the ligand remains in monomer B, all along the simulation with poses close to the predicted docked complex and strong interaction with the catalytic binding site, monomer A displaces its ligand at about 200 ns, which then remains closer to the entrance of the monomer-binding site. This displacement toward more solvent exposed location of monomer A is more pronounced for proanthocyanidin B2 than cadambine (Figures S3 and S4). Therefore, cadambine and proanthocyanidin B2 seem to lead to one very stable binding with associated conformational changes that relate, in an apparent allosteric manner, on the second one.

These structural observations were further quantified by MM-GBSA analysis (Table 2). Results show that $\Delta G_{\text{binding}}$ of the species in the different monomers range from ca. -52 kcal/mol to ca. -15 kcal/mol. Taking average values between S1_A and S1_B sites, the affinity of the different phytochemical compounds to 3CL^{PRO} can be classified as cadambine (approx. -40 kcal/mol) > speciophylline (approx. -35 kcal/mol) > proanthocyanidin (approx. -20 kcal/mol). These values suggest the two former molecules to be good binders to 3CL^{PRO} and the latest to be somehow of lesser quality. When analyzing each monomer individually, the $\Delta G_{\text{binding}}$ values are consistent with the structural observation with speciophylline having almost symmetric values (ca. -33 kcal/mol) and cadambine and proanthocyanidin having different magnitudes. The closer energy values for cadambine and speciophylline are consistent with the structural similarities between both alkaloids with respect to proanthocyanidin.

In the light of the molecular dynamics analysis and the calculation of the free energy of binding, at least cadambine and speciophylline are predicted to present very good inhibition to the SARS-CoV-2 main protease. Because these components are found in the ethanolic extract of Cat's claw, it may position itself as possible therapeutic herbal for COVID-19.

3.5. Calculation of Drug-Likeness Indices and Scoring. Calculated human pharmacokinetics profiles play a critical role in assessing the quality of novel antiviral candidates. Early predictions of pharmacokinetic behavior of the promising antiviral compounds based on their structure could help finding safer and effective leads for preclinical antiviral testing. Herein, we calculated and analyzed various drug-likeness indices for the most qualified Cat's claw components (Table 3). Ten pharmacokinetics parameters were calculated as a drug-likeness filter for speciophylline, cadambine, and proanthocyanidin B2 and compared to N3 and three selected antiviral drugs. Results obtained demonstrate the feasibility of the selected components from Cat's claw exhibiting suitable drug-like characteristics.

In addition, lipophilicity (calculated as $\log P_{o/w}$) is the key physicochemical property for rational drug design. This parameter provides valuable information about transport through lipid bilayers. Compounds that display high $\log P_{o/w}$ tend to have good permeability across the cell wall [66, 67]. In this study, the selected compounds exhibited optimal $\log P_{o/w}$ values < 6.5; notably speciophylline has a $\log P_{o/w}$ of 1.709 (optimal value compared to 95% of current drugs) implying good permeability across the cell membrane of infected cells. Furthermore, the *in silico* passive transmembrane permeation was calculated for all compounds using Caco-2 cell monolayers or MDCK cells as a model. Cadambine and proanthocyanidin B2 exhibit low values of permeability (<27 nm/s), clearly suggesting poor bioavailability [88]. However, an optimal value for the alkaloid speciophylline was predicted (307 nm/s for Caco-2 model) close to ritonavir and lopinavir drugs [89–91] and was much better than the inhibitor N3 (6 nm/s for Caco-2 model).

Finally, binding to serum albumin (expressed as $\log K_{\text{HSA}}$) is the most important parameter for distribution and transport of antiviral drugs in the systemic circulation. Early prediction of this parameter reduces the amount of wasted time and resources for drug development candidates in the

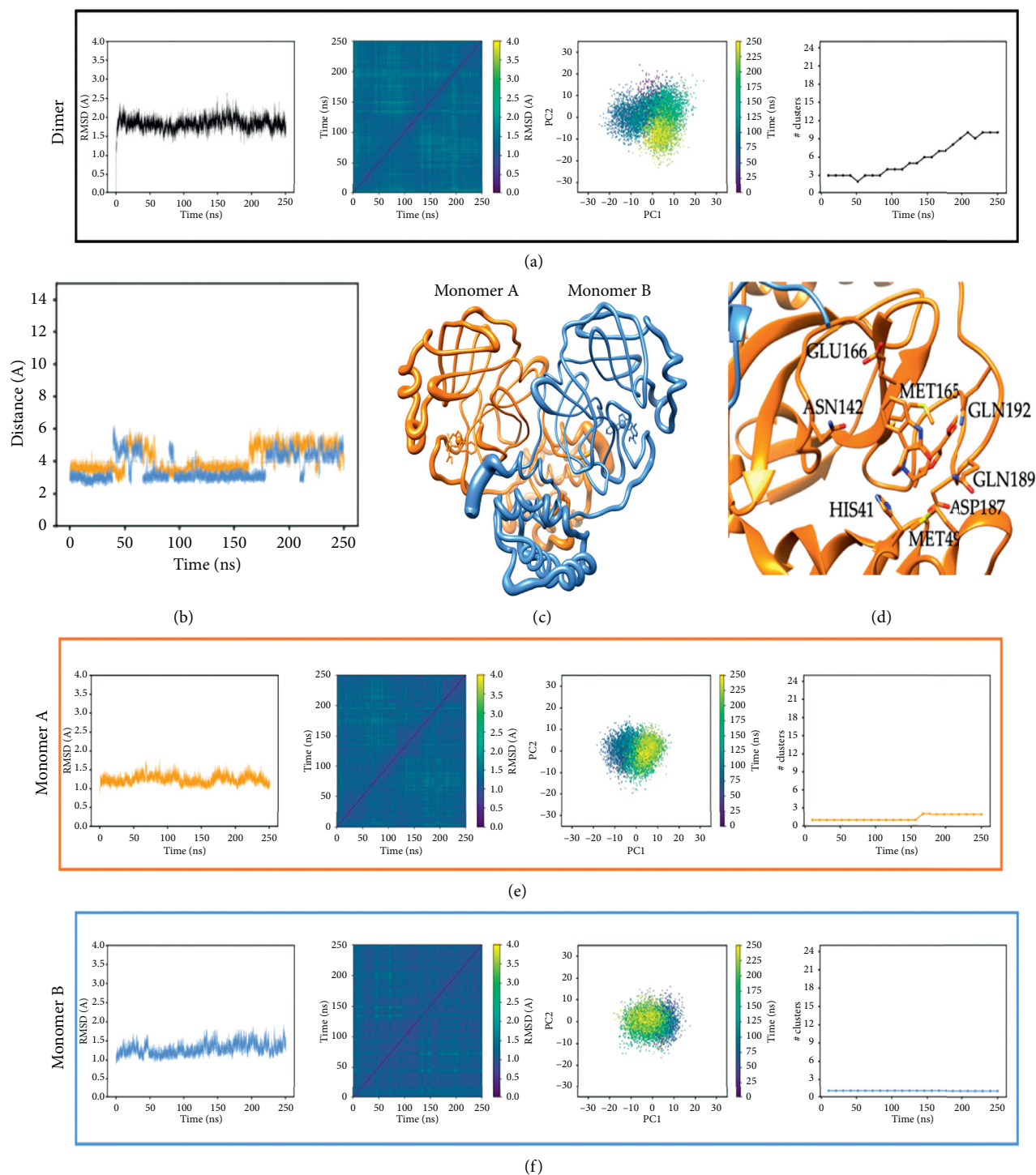


FIGURE 5: Complete analysis of the 250 ns trajectory of 3CLP^D of SARS-CoV-2 bound with speciophylline. Monomer A is shown in orange and monomer B in blue. (a), (e), and (f) shows, from left to right, RMSD, all-to-all RMSD, PCA, and cluster counting (cutoff 1.5 Å). (b) shows the relative position of speciophylline molecules versus the center of mass of the S1 cavity along the simulation (black dashed line indicates the distance of the N3 inhibitor as reference). In (c), size of the ribbon is proportional to the flexibility of the protein backbone and the size on the ligand center is proportional to the amount of structural deviation of the ligand during the 250 ns. (d) reproduces the binding site S1 with the most important residues involved in the interactions.

antiviral therapy and management. Behavior of the selected compounds with human plasma protein ($\log K_{HSA}$) is within recommended values (ranging from -0.30 to -0.044)

compared to the reference value taken from 95% of currently known drugs ($\log K_{HSA}$ from -1.5 to 2.0). Optimal physicochemical properties obtained for the active components of

TABLE 2: Ligand-protease $\Delta G_{\text{binding}}$ in kcal/mol.

	Cadambine	Proanthocyanidin B2	Speciophylline
Monomer B	-51.92 ± 6.03	-21.20 ± 6.22	-33.49 ± 4.88
Monomer A	-32.25 ± 5.84	-15.25 ± 7.31	-33.34 ± 6.15

The average obtained from 250 frames for each MD trajectory (one per nanosecond) using the MM-GBSA method in AmberTools18. The following parameters were used: $\text{igb} = 2$, $\text{saltcon} = 0.100$.

TABLE 3: Calculated drug-likeness properties of the most qualified Cat's claw components.

Compound	MW ^a	PSA ^b	n-Rot Bond (0-10)	n-ON (<10) ^c	n-OHNH ^d	Log $P_{o/w}$ ^e	Log K_{HSA} ^f	Caco-2 ^g (nm/s)	App. MDCK (nm/s) ^h	% HIA ⁱ	Lipinski rule of five (≤ 1)
Speciophylline	368.432	82.804	1	8	1	1.709	-0.044	307	153	81	0
Cadambine	544.557	158.806	8	11	5	0.037	-0.592	27	11	27	0
Proanthocyanidin B2	578.528	209.177	10	12	10	0.505	-0.300	1	1	<25	1
N3	680.800	221.219	17	14	3	2.578	-0.497	6	11	85	2
Remdesivir ^j	602.583	196.086	16	16	5	1.135	-0.685	37	14	36	2
Ritonavir ^j	720.943	139.542	18	11	3	6.335	0.638	647	1014	75	2
Lopinavir ^j	628.810	124.690	16	9	4	5.751	0.554	510	598	83	2

^aMolecular weight of the hybrid (150–500). ^bPolar surface area (PSA) (7.0–200 Å²). ^cn-ON number of hydrogen bond acceptors <10. ^dn-OHNH number of hydrogen bond donors ≤ 5 . ^eOctanol water partition coefficient (log $P_{o/w}$) (-2.0 to 6.5). ^fBinding-serum albumin (K_{HSA}) (-1.5 to 1.5). ^gHuman intestinal permeation (<25 poor, >500 great). ^hMadin-Darby canine kidney (MDCK) cell permeation. ⁱHuman intestinal absorption (% HIA) (>80% is high, <25% is poor). ^jFDA-approved antiviral drugs used as references.

Cat's claw indicated that this herb should be considered for the rapid progression in the antiviral treatment.

4. Conclusions

The coronavirus pandemic is a serious public health crisis due to high mortality, high basic reproduction numbers, and neither approved drugs nor vaccines. The recent publication of the crystal structure of the SARS-CoV-2 main protease has provided the community with critical structural information. Potential inhibitors of this enzyme could have a major contribution in the reduction, prevention, or eradication of the viral load of patients.

This study aimed at computationally explore if *Uncaria tomentosa* (Cat's claw), an indigenous medicinal herb known for its antiviral properties against other high mortality viruses, contains phytochemicals potentially able to inhibit the SARS-CoV-2 main protease, 3CL^{Pro}.

After screening 26 key compounds of *Uncaria tomentosa* against the 3CL^{Pro} cleavage site, nine compounds displayed lower binding energies than those of known inhibitors of this enzyme (N3 as well as three FDA-approved antiviral drugs). Amongst those nine compounds, one of each family of well-characterized active phytochemical fractions of Cat's claw, namely, speciophylline, cadambine, and proanthocyanidin B2, attracted our attention because of their strong docking scores (-8.1, -8.6, and -9.2 kcal/mol, respectively). The potential inhibitory effects of those molecules were further analyzed by means of ligand pathway simulations (which show very low barriers for binding), molecular dynamics of the docked complexes (until convergence at approx. 250 ns), and MM-GBSA free energy binding calculations (with values ranging from ca. -50 kcal/mol to ca. -15 kcal/mol). Altogether, these results confirm that the three compounds, and more particularly the alkaloid ones, have

good predicted inhibitory profiles. To anticipate the therapeutic behavior of Cat's claw components, several physicochemical and ADME-score indices were calculated using themore activemolecules and compared to antiviral marketed drugs. The returned values show optimal drug-like properties for speciophylline, cadambine, and proanthocyanidin B2.

Due to the remarkable presence of these compounds in the Cat's claw extracts, we believe that this *in silico* study at least points at *Uncaria tomentosa* as a whole as an interesting herb opening novel therapeutically horizons for COVID-19 treatment. Based on our findings, we believe that Cat's claw should be taken into consideration in looking for COVID-19 treatments.

Abbreviations

PCA:	Principal component analysis
ADME:	Absorption, distribution, metabolism, and excretion
MD:	Molecular dynamics
FDA:	Food and Drug Administration
TNF α :	Tumor necrosis factor alpha
EsSalud:	Seguro Social de Salud (in Spanish)
PDB:	Protein Data Bank.

Data Availability

All data used to support the findings of this study can be made available from the corresponding author upon request.

Conflicts of Interest

The authors declare no conflicts of interest.

Authors' Contributions

O.H.-C. and A.F.Y.-P. conceptualized the study; A.F.Y.-P. and J.-D.M. developed the methodology; A.F.Y.-P., J.-E.S.-A., and L.T.-S. were responsible for software; W.C.-G. and J.-D.M. validated the results; J.-D.M. performed the formal analysis; O.H.-C. and A.F.Y.-P. were involved in investigation; W.C.-G. was responsible for data curation; O.H.-C., A.F.Y.-P., J.D.M., and J.-E.S.-A. were involved in writing and editing and original draft preparation; A.F.Y.-P., L.T.-S., and J.D.-M. were involved in review and editing of the manuscript; W.C.-G. was involved in visualization; A.F.Y.-P. supervised the study. All authors have read and agreed to the published version of the manuscript.

Acknowledgments

J.-E.S.-A., L.T.-S., and J.-D.M. gratefully acknowledge the financial support from the Spanish MINECO (CTQ2017-87889-P). The authors would like to thank Universidad de Antioquia, Universidad Nacional Mayor de San Marcos, and Universitat Autònoma de Barcelona.

Supplementary Materials

Figure S1: histogram showing molecular docking results between the novel SARS-CoV-2 main protease and nine components from Cat's claw which showed the highest binding affinity. Figure S2: (A) the best conformation of the nine active components inside the catalytic pocket of the SARS-CoV-2 main protease 3CL^{PRO} (PDB: 6LU7). 2D interaction mode plots of the selected compounds with 3CL^{PRO}. Interactions between each component and amino acid residues inside the 3CL^{PRO} cleavage domain are indicated by the dashed lines. Figure S3: complete analysis of the 250 ns trajectory of 3CL^{PRO} of SARS-CoV-2 bound with cadambine. Monomer A is shown in orange and monomer B in blue. Panels A, E, and F show, from left to right, RMSD, all-to-all RMSD, PCA, and cluster counting (cutoff 1.5 Å). Panel B shows the relative position of cadambine molecules versus the center of mass of the S1 cavity along the simulation (black dashed line indicates the distance of the N3 inhibitor as reference). For panel C, size of the ribbon is proportional to the flexibility of the protein backbone and the size on the ligand center is proportional to the amount of structural deviation of the ligand during the 250 ns. Panel D reproduces the binding site S1 with the most important residues involved in the interactions. Figure S4: complete analysis of the 250 ns trajectory of 3CL^{PRO} of SARS-CoV-2 bound with proanthocyanidin B2. Monomer A is shown in orange and monomer B in blue. Panels A, E, and F shows, from left to right, RMSD, all-to-all RMSD, PCA, and cluster counting (cutoff 1.5 Å). Panel B shows the relative position of proanthocyanidin B2 molecules versus the center of mass of the S1 cavity along the simulation (black dashed line indicates the distance of the N3 inhibitor as reference). For panel C, size of the ribbon is proportional to the flexibility of the protein backbone and the size on the ligand center is proportional to the amount of structural deviation of the

ligand during the 250 ns. Panel D reproduces the binding site S1 with the most important residues involved in the interactions. Table S1: GPathFinder vina barriers for the ligand route. 120 solutions were obtained for each ligand. Average and standard deviation are reported. Table S2: amino acids of the 3CL^{PRO} protease that participate in hydrogen bonding interactions with cadambine, proanthocyanidin B2, and speciohylline. Input file (.yaml format) used in Gpath-Finder calculations. (*Supplementary Materials*)

References

- [1] T. Singhal, "A review of coronavirus disease-2019 (COVID-19)," *Indian Journal of Pediatrics*, vol. 87, no. 4, pp. 281–286, 2020.
- [2] Y. W. Chen, C. P. B. Yiu, and K. Y. Wong, "Prediction of the SARS-CoV-2 (2019-nCoV) 3C-like protease (3CLpro) structure: virtual screening reveals velpatasvir, ledipasvir, and other drug repurposing candidates," *F1000 Research*, vol. 9, p. 129, 2020.
- [3] C. Wang, P. W. Horby, F. G. Hayden, and G. F. Gao, "A novel coronavirus outbreak of global health concern," *The Lancet*, vol. 395, no. 10223, pp. 470–473, 2020.
- [4] J. Williamson, R. Ramirez, and T. Wingfield, "Health, healthcare access, and use of traditional versus modern medicine in remote Peruvian Amazon communities: a descriptive study of knowledge, attitudes, and practices," *The American Journal of Tropical Medicine and Hygiene*, vol. 92, no. 4, pp. 857–864, 2015.
- [5] R. W. Bussmann, G. Malca-García, A. Glenn et al., "Minimum inhibitory concentrations of medicinal plants used in Northern Peru as antibacterial remedies," *Journal of Ethnopharmacology*, vol. 132, no. 1, pp. 101–108, 2010.
- [6] S. Ben-Shabat, L. Yarmolinsky, D. Porat, and A. Dahan, "Antiviral effect of phytochemicals from medicinal plants: applications and drug delivery strategies," *Drug Delivery and Translational Research*, vol. 10, no. 2, pp. 354–367, 2020.
- [7] O. Herrera-Calderon, J. L. Arroyo-Acevedo, J. Rojas-Armas et al., "Phytochemical screening, total phenolic content, antioxidant and cytotoxic activity of *Chromolaena laevigata* on human tumor cell lines," *Annual Research & Review in Biology*, vol. 21, no. 1, pp. 1–9, 2017.
- [8] M. E. Heitzman, C. C. Neto, E. Winiarz, A. J. Vaisberg, and G. B. Hammond, "Ethnobotany, phytochemistry and pharmacology of *Uncaria* (Rubiaceae)," *ChemInform*, vol. 36, no. 17, 2005.
- [9] K. Keplinger, G. Laus, M. Wurm, M. P. Dierich, and H. Teppner, "*Uncaria tomentosa* (Willd.) DC.—ethnomedicinal use and new pharmacological, toxicological and botanical results," *Journal of Ethnopharmacology*, vol. 64, no. 1, pp. 23–34, 1998.
- [10] G. F. Gonzales, J. Aguilar, and M. Villar, "The world summit of harmonization on traditional, alternative and complementary medicine (TACM) in Lima, Peru," *Evidence-based Complementary and Alternative Medicine*, vol. 7, no. 2, pp. 271–275, 2010.
- [11] A. Kośmider, E. Czepielewska, M. Kuraś et al., "*Uncaria tomentosa* leaves decoction modulates differently ROS production in cancer and normal cells, and effects cisplatin cytotoxicity," *Molecules*, vol. 22, no. 4, p. 620, 2017.
- [12] S. Zhu, Q. Li, S. Chen et al., "Phylogenetic analysis of *Uncaria* species based on internal transcribed spacer (ITS) region and

- ITS2 secondary structure,” *Pharmaceutical Biology*, vol. 56, no. 1, pp. 548–558, 2018.
- [13] A. D. Snow, G. M. Castillo, B. P. Nguyen et al., “The Amazon rain forest plant *Uncaria tomentosa* (cat’s claw) and its specific proanthocyanidin constituents are potent inhibitors and reducers of both brain plaques and tangles,” *Scientific Reports*, vol. 9, no. 1, 2019.
- [14] G. Laus, D. Brössner, and K. Keplinger, “Alkaloids of Peruvian *Uncaria tomentosa*,” *Phytochemistry*, vol. 45, no. 4, pp. 855–860, 1997.
- [15] I. Vera-Reyes, A. A. Huerta-Heredia, T. Ponce-Noyola et al., “Monoterpenoid indole alkaloids and phenols are required antioxidants in glutathione depleted *Uncaria tomentosa* root cultures,” *Frontiers in Environmental Science*, vol. 3, 2015.
- [16] P. Montoro, V. Carbone, J. de Dioz Zuniga Quiroz, F. De Simone, and C. Pizza, “Identification and quantification of components in extracts of *Uncaria tomentosa* by HPLC-ES/MS,” *Phytochemical Analysis*, vol. 15, no. 1, pp. 55–64, 2004.
- [17] R. Aquino, N. De Tommasi, F. De Simone, and C. Pizza, “Triterpenes and quinovic acid glycosides from *Uncaria tomentosa*,” *Phytochemistry*, vol. 45, no. 5, pp. 1035–1040, 1997.
- [18] R. Cerri, R. Aquino, F. De Simone, and C. Pizza, “New quinovic acid glycosides from *Uncaria tomentosa*,” *Journal of Natural Products*, vol. 51, no. 2, pp. 257–261, 1988.
- [19] E. M. C. Peñaloza, S. Kaiser, P. E. De Resende et al., “Chemical composition variability in the *Uncaria tomentosa* (cat’s claw) wild population,” *Química Nova*, vol. 38, no. 3, 2015.
- [20] M. N. Hoyos, F. Sánchez-Patán, R. M. Masis et al., “Phenolic assessment of *Uncaria tomentosa* L. (cat’s claw): leaves, stem, bark and wood extracts,” *Molecules*, vol. 20, no. 12, pp. 22703–22717, 2015.
- [21] M. Kitajima, K. I. Hashimoto, M. Yokoya, H. Takayama, and N. Aimi, “Two new 19-hydroxyursolic acid-type triterpenes from Peruvian ‘Una de Gato’ (*Uncaria tomentosa*),” *Tetrahedron*, vol. 56, no. 4, pp. 547–552, 2000.
- [22] A. M. P. Yépez, O. L. de Ugaz, C. M. P. Alvarez et al., “Quinovic acid glycosides from *Uncaria guianensis*,” *Phytochemistry*, vol. 30, no. 5, pp. 1635–1637, 1991.
- [23] R. Aquino, F. De Simone, C. Pizza, C. Conti, and M. L. Stein, “Plant metabolites. Structure and in vitro antiviral activity of quinovic acid glycosides from *Uncaria tomentosa* and *Guettarda platypoda*,” *Journal of Natural Products*, vol. 52, no. 4, pp. 679–685, 1989.
- [24] J. Yunis Aguinaga, G. S. Claudiano, P. F. Marcusso et al., “Acute toxicity and determination of the active constituents of aqueous extract of *Uncaria tomentosa* bark in *Hyphessobrycon eques*,” *Journal of Toxicology*, vol. 2014, Article ID 412437, 5 pages, 2014.
- [25] S. R. I. N. Reis, L. M. M. Valente, A. L. Sampaio et al., “Immunomodulating and antiviral activities of *Uncaria tomentosa* on human monocytes infected with dengue virus-2,” *International Immunopharmacology*, vol. 8, no. 3, pp. 468–476, 2008.
- [26] R. S. Lima-Junior, C. Da Silva Mello, C. F. Kubelka, A. C. Siani, and L. M. M. Valente, “*Uncaria tomentosa* alkaloidal fraction reduces paracellular permeability, IL-8 and NS1 production on human microvascular endothelial cells infected with dengue virus,” *Natural Product Communications*, vol. 8, no. 11, Article ID 1934578X1300801, 2013.
- [27] T. Caon, S. Kaiser, C. Feltrin et al., “Antimutagenic and antiherpetic activities of different preparations from *Uncaria tomentosa* (cat’s claw),” *Food and Chemical Toxicology*, vol. 66, pp. 30–35, 2014.
- [28] L. Allen-Hall, J. T. Arnason, P. Cano, and R. M. Lafrenie, “*Uncaria tomentosa* acts as a potent TNF- α inhibitor through NF- κ B,” *Journal of Ethnopharmacology*, vol. 127, no. 3, pp. 685–693, 2010.
- [29] J. E. Williams, “Review of antiviral and immunomodulating properties of plants of the Peruvian rainforest with a particular emphasis on uña de gato and sangre de grado,” *Alternative Medicine Review*, vol. 6, no. 6, pp. 567–579, 2001.
- [30] M. Sandoval, R. M. Charbonnet, N. N. Okuhama et al., “Cat’s claw inhibits TNF α production and scavenges free radicals: role in cytoprotection,” *Free Radical Biology and Medicine*, vol. 29, no. 1, pp. 71–78, 2000.
- [31] R. M. López Galera, E. Ribera Pascuet, J. I. Esteban Mur, J. B. Montoro Ronsano, and J. C. Juárez Giménez, “Interaction between cat’s claw and protease inhibitors atazanavir, ritonavir and saquinavir,” *European Journal of Clinical Pharmacology*, vol. 64, no. 12, pp. 1235–1236, 2008.
- [32] C. Åkesson, R. W. Pero, and F. Ivars, “C-Med 100®, a hot water extract of *Uncaria tomentosa*, prolongs lymphocyte survival in vivo,” *Phytomedicine*, vol. 10, no. 1, pp. 23–33, 2003.
- [33] S. L. Chen, H. Yu, H. M. Luo et al., “Conservation and sustainable use of medicinal plants: problems, progress, and prospects,” *Chinese Medicine (United Kingdom)*, vol. 11, no. 1, 2016.
- [34] M. Prajapat, P. Sarma, N. Shekhar et al., “Drug targets for corona virus: a systematic review,” *Scholars International Journal of Biochemistry*, vol. 3, no. 6, pp. 143–153, 2020.
- [35] C. Wu, Y. Liu, Y. Yang et al., “Analysis of therapeutic targets for SARS-CoV-2 and discovery of potential drugs by computational methods,” *Acta pharmaceutica Sinica. B*, vol. 10, no. 5, pp. 766–788, 2020.
- [36] A. D. Elmezayen, A. Al-Obaidi, A. T. Şahin, and K. Yeleği, “Drug repurposing for coronavirus (COVID-19): in silico screening of known drugs against coronavirus 3CL hydrolase and protease enzymes,” *Journal of Biomolecular Structure and Dynamics*, vol. 1–13, 2020.
- [37] K. A. Peele, C. Potla Durthi, T. Srihansa et al., “Molecular docking and dynamic simulations for antiviral compounds against SARS-CoV-2: a computational study,” *Informatics in Medicine Unlocked*, vol. 19, Article ID 100345, 2020.
- [38] G. M. Morris, D. S. Goodsell, R. S. Halliday et al., “Automated docking using a Lamarckian genetic algorithm and an empirical binding free energy function,” *Journal of Computational Chemistry*, vol. 19, no. 14, pp. 1639–1662, 1998.
- [39] Q. Wang, Y. Zhao, X. Chen, and A. Hong, “Virtual screening of approved clinic drugs with main protease (3CLpro) reveals potential inhibitory effects on SARS-CoV-2,” *Journal of Biomolecular Structure and Dynamics*, pp. 1–11, 2020.
- [40] L. Zhang, D. Lin, X. Sun et al., “Crystal structure of SARS-CoV-2 main protease provides a basis for design of improved α -ketoamide inhibitors,” *Science*, vol. 368, no. 6489, pp. 409–412, 2020.
- [41] Z. Jin, X. Du, Y. Xu et al., “Structure of Mpro from SARS-CoV-2 and discovery of its inhibitors,” *Nature*, vol. 582, no. 7811, pp. 289–293, 2020.
- [42] N. Fintelman-Rodrigues, C. Q. Sacramento, C. R. Lima et al., “Atazanavir inhibits SARS-CoV-2 replication and pro-inflammatory cytokine production,” 2020.
- [43] D. L. McKee, A. Sternberg, U. Stange, S. Laufer, and C. Naujokat, “Candidate drugs against SARS-CoV-2 and COVID-19,” *Pharmacological Research*, vol. 157, Article ID 104859, 2020.

- [44] M. A. Martinez, "Compounds with therapeutic potential against novel respiratory 2019 coronavirus," *Antimicrobial Agents and Chemotherapy*, vol. 64, no. 5, Article ID e00399, 2020.
- [45] A. T. Ton, F. Gentile, M. Hsing, F. Ban, and A. Cherkasov, "Rapid identification of potential inhibitors of SARS-CoV-2 main protease by deep docking of 1.3 billion compounds," *Molecular Informatics*, vol. 39, no. 8, Article ID e2000028, 2020.
- [46] S. Jo, S. Kim, D. H. Shin, and M. S. Kim, "Inhibition of SARS-CoV 3CL protease by flavonoids," *Journal of Enzyme Inhibition and Medicinal Chemistry*, vol. 35, no. 1, pp. 145–151, 2020.
- [47] Z. Haider, M. M. Subhani, M. A. Farooq et al., "In silico discovery of novel inhibitors against main protease (Mpro) of SARS-CoV-2 using pharmacophore and molecular docking based virtual screening from ZINC database," 2020.
- [48] ChemAxon, *ChemAxon—Software Solutions and Services for Chemistry and Biology (Version 16.10.31)*, ChemAxon, Budapest, Hungary, 2016.
- [49] O. Trott and A. J. Olson, "AutoDock Vina: improving the speed and accuracy of docking with a new scoring function, efficient optimization, and multithreading," *Journal of Computational Chemistry*, vol. 31, no. 2, pp. 455–461, 2010.
- [50] Schrödinger, "PyMOL, molecular visualization system," 2018, <https://pymol.org>.
- [51] J. E. Sánchez-Aparicio, G. Sciortino, D. V. Herrmannsdoerfer et al., "Gpathfinder: identification of ligand-binding pathways by a multi-objective genetic algorithm," *International Journal of Molecular Sciences*, vol. 20, no. 13, p. 3155, 2019.
- [52] R. González-Alemán, D. Hernández-Castillo, J. Caballero, and L. A. Montero-Cabrera, "Quality threshold clustering of molecular dynamics: a word of caution," *Journal of Chemical Information and Modeling*, vol. 60, no. 2, pp. 467–472, 2020.
- [53] H. M. Berman, J. Westbrook, Z. Feng et al., "The Protein Data Bank (www.rcsb.org)," *Nucleic Acids Research*, vol. 28, no. 1, pp. 235–242, 2000.
- [54] E. F. Pettersen, T. D. Goddard, C. C. Huang et al., "UCSF Chimera—a visualization system for exploratory research and analysis," *Journal of Computational Chemistry*, vol. 25, no. 13, pp. 1605–1612, 2004.
- [55] L. F. Song, T. S. Lee, C. Zhu, D. M. York, and K. M. Merz, "Using AMBER18 for relative free energy calculations," *Journal of Chemical Information and Modeling*, vol. 59, no. 7, pp. 3128–3135, 2019.
- [56] M. J. Frisch, G. W. Trucks, H. B. Schlegel et al., *Gaussian 09, Revision B.01*, Gaussian, Inc., Wallingford, CT, USA, 2009.
- [57] C. I. Bayly, P. Cieplak, W. D. Cornell, and P. A. Kollman, "A well-behaved electrostatic potential based method using charge restraints for deriving atomic charges: the RESP model," *The Journal of Physical Chemistry*, vol. 97, no. 40, pp. 10269–10280, 1993.
- [58] D. A. Case, I. Y. Ben-Shalom, S. R. Brozell et al., "Amber 2018," 2018.
- [59] P. Eastman, J. Swails, J. D. Chodera et al., "OpenMM 7: rapid development of high performance algorithms for molecular dynamics," *PLoS Computational Biology*, vol. 13, no. 7, Article ID e1005659, 2017.
- [60] J. Rodríguez-Guerra Pedregal, L. Alonso-Cotchico, L. Velasco-Carneros, and J.-D. Maréchal, "OMMProtocol: a command line application to launch molecular dynamics simulations with OpenMM," 2018.
- [61] J. D. Irvine, L. Takahashi, K. Lockhart et al., "MDCK (Madin-Darby canine kidney) cells: a tool for membrane permeability screening," *Journal of Pharmaceutical Sciences*, vol. 88, no. 1, pp. 28–33, 1999.
- [62] Calculation of Molecular Properties and Bioactivity Score Software, Molinspiration Cheminformatics, 2020, <http://www.molinspiration.com/cgi-bin/properties>.
- [63] I. V. Tetko and G. I. Poda, "Application of ALOGPS 2.1 to predict log D distribution coefficient for Pfizer proprietary compounds," *Journal of Medicinal Chemistry*, vol. 47, no. 23, pp. 5601–5604, 2004.
- [64] F. Broccatelli, L. Salphati, E. Plise et al., "Predicting passive permeability of drug-like molecules from chemical structure: where are we?" *Molecular Pharmaceutics*, vol. 13, no. 12, pp. 4199–4208, 2016.
- [65] H. Yang, C. Lou, L. Sun et al., "AdmetSAR 2.0: web-service for prediction and optimization of chemical ADMET properties," *Bioinformatics*, vol. 35, no. 6, pp. 1067–1069, 2019.
- [66] I. J. Flores-Sánchez, J. Ortega-López, M. D. C. Montes-Horcasitas, and A. C. Ramos-Valdivia, "Biosynthesis of sterols and triterpenes in cell suspension cultures of *Uncaria tomentosa*," *Plant and Cell Physiology*, vol. 43, no. 12, pp. 1502–1509, 2002.
- [67] M. Navarro, W. Zamora, S. Quesada et al., "Fractioning of proanthocyanidins of *Uncaria tomentosa*. Composition and structure-bioactivity relationship," *Antioxidants*, vol. 6, no. 3, p. 60, 2017.
- [68] M. Navarro, E. Arnaez, I. Moreira et al., "Polyphenolic composition and antioxidant activity of *Uncaria tomentosa* commercial bark products," *Antioxidants*, vol. 8, no. 9, p. 339, 2019.
- [69] M. D. C. Santos Araújo, I. L. Farias, J. Gutierrez et al., "Uncaria tomentosa—adjuvant treatment for breast cancer: clinical trial," *Evidence-Based Complementary and Alternative Medicine*, vol. 2012, Article ID 676984, 8 pages, 2012.
- [70] L. C. L. De Paula, F. Fonseca, F. Perazzo et al., "Uncaria tomentosa (Cat's claw) improves quality of life in patients with advanced solid tumors," *The Journal of Alternative and Complementary Medicine*, vol. 21, no. 1, pp. 22–30, 2015.
- [71] C. Gonçalves, T. Dinis, and M. T. Batista, "Antioxidant properties of proanthocyanidins of *Uncaria tomentosa* bark decoction: a mechanism for anti-inflammatory activity," *Phytochemistry*, vol. 66, no. 1, pp. 89–98, 2005.
- [72] O. Lock, E. Perez, M. Villar, D. Flores, and R. Rojas, "Bioactive compounds from plants used in Peruvian traditional medicine," *Natural Product Communications*, vol. 11, no. 3, pp. 315–337, 2016.
- [73] R. T. Brown, D. M. Duckworth, and C. A. M. Santos, "Biogenetically patterned synthesis of cadambine," *Tetrahedron Letters*, vol. 32, no. 17, pp. 1987–1990, 1991.
- [74] D. Pierrot, V. Sinou, S. S. Bun et al., "Design and synthesis of simplified speciophylline analogues and β -carbolines as active molecules against *Plasmodium falciparum*," *Drug Development Research*, vol. 80, no. 1, pp. 133–137, 2019.
- [75] W. Fujii, K. Toda, K. Matsumoto et al., "Syntheses of prodelphinidin B1, B2, and B4 and their antitumor activities against human PC-3 prostate cancer cell lines," *Tetrahedron Letters*, vol. 54, no. 52, pp. 7188–7192, 2013.
- [76] P. Rasoanaivo, C. W. Wright, M. L. Willcox, and B. Gilbert, "Whole plant extracts versus single compounds for the treatment of malaria: synergy and positive interactions," *Malaria Journal*, vol. 10, no. S1, 2011.
- [77] S. Khaerunnisa, H. Kurniawan, R. Awaluddin, and S. Suhartati, "Potential inhibitor of COVID-19 main protease (M^{Pro}) from several medicinal plant compounds by molecular docking study," 2020.

- [78] C. Navan, "Possible drug candidates for COVID-19," 2020.
- [79] K. Gao, D. D. Nguyen, R. Wang, and G.-W. Wei, "Machine intelligence design of 2019-nCoV drugs," 2020.
- [80] L. Mittal, A. Kumari, M. Srivastava, M. Singh, and S. Asthana, "Identification of potential molecules against COVID-19 main protease through structure-guided virtual screening approach," *Journal of Biomolecular Structure and Dynamics*, pp. 1–19, 2020.
- [81] Y. Kumar, H. Singh, and C. N. Patel, "In silico prediction of potential inhibitors for the main protease of SARS-CoV-2 using molecular docking and dynamics simulation based drug-repurposing," *Journal of Infection and Public Health*, vol. 13, no. 9, pp. 1210–1223, 2020.
- [82] X. Wang, R. S. Dhindsa, G. Povysil et al., "Transcriptional inhibition of host viral entry proteins as a therapeutic strategy for SARS-CoV-2," 2020.
- [83] H. Amawi, G. I. Abu Deiab, A. A. A. Aljabali, K. Dua, and M. M. Tambuwala, "COVID-19 pandemic: an overview of epidemiology, pathogenesis, diagnostics and potential vaccines and therapeutics," *Therapeutic Delivery*, vol. 11, no. 4, pp. 245–268, 2020.
- [84] S. M. Lipson, G. Karalis, L. Karthikeyan et al., "Mechanism of anti-rotavirus synergistic activity by epigallocatechin gallate and a proanthocyanidin-containing nutraceutical," *Food and Environmental Virology*, vol. 9, no. 4, pp. 434–443, 2017.
- [85] C. S. Lupala, X. Li, J. Lei et al., "Computational simulations reveal the binding dynamics between human ACE2 and the receptor binding domain of SARS-CoV-2 spike protein," 2020.
- [86] P. Eastman and V. S. Pande, "OpenMM: a hardware-independent framework for molecular simulations," *Computing in Science & Engineering*, vol. 12, no. 4, pp. 34–39, 2010.
- [87] L. Alonso-Cotchico, J. R. G. Pedregal, A. Lledós, and J. D. Maréchal, "The effect of cofactor binding on the conformational plasticity of the biological receptors in Artificial Metalloenzymes: the case study of LmrR," *Frontiers in Chemistry*, vol. 7, 2019.
- [88] C. A. Lipinski, F. Lombardo, B. W. Dominy, and P. J. Feeney, "Experimental and computational approaches to estimate solubility and permeability in drug discovery and development settings," *Advanced Drug Delivery Reviews*, vol. 64, pp. 4–17, 2012.
- [89] J. T. Ortega, M. L. Serrano, F. H. Pujol, and H. R. Rangel, "Unrevealing sequence and structural features of novel coronavirus using in silico approaches: the main protease as molecular target," *EXCLI Journal*, vol. 19, 2020.
- [90] G. A. Gyebi, O. B. Ogunro, A. P. Adegunloye, O. M. Ogunyemi, and S. O. Afolabi, "Potential inhibitors of coronavirus 3-chymotrypsin-like protease (3CLpro): an in silico screening of alkaloids and terpenoids from African medicinal plants," *Journal of Biomolecular Structure and Dynamics*, pp. 1–13, 2020.
- [91] C. J. Dennis, L. Bruno, D. Rodrigo et al., "Antiretroviral drug activity and potential for pre-exposure prophylaxis against COVID-19 and HIV infection," 2020.